3D simulation of hybrid Fabry-Pérot for single mode fibre

Jean Bittebierre, Jérôme Felder

3D Simulation of Hybrid Fabry-Pérot for Single Mode Fibre

Jean Bittebierre*, Jérôme Felder

Aix Marseille Univ, CNRS, Centrale Marseille, Institut Fresnel, 13013 Marseille, France

*Corresponding author : jean.bittebierre@centrale-marseille.fr

Dr Jean Bittebierre, Institut Fresnel, Faculté des Sciences de Saint Jérôme, Avenue Escadrille Normandie-Niemen, 13397 Marseille CEDEX, France

Abstract

3D modal simulation of **Hybrid Fabry Pérot** (**H-FP**) consisting of a Bragg grating (**Bg**) and a multilayer mirror between single-mode optical fibres shows that diffraction in their multilayer is negligible, but that multimode **3D S**-matrix calculation is essential in the multilayer to determine the adequate thickness of the interface layer with the **Bg**. The single-mode approximation made in **1D** calculation is justified for their sinusoidal profile **Bg**, but is not at the top of the transmission peak for their high step profile **Bg**. The study of manufacturing constraints shows that feasible **H-FP**s, with rejection broad of several hundred nanometers, provide access to bandpass widths as low as 15 fm, but that the control of the bandwidth shift remains delicate for the realization of large series. The principle of **H-FP** with a high refraction index step reflector and a low step one is also valid for integrated optics. All weak spectral oscillations in the rejection band of **H-FPs** have been interpreted. Finally, the simulation of **H-FPs** with Interleaved Fibre (**IF**) between their 2 mirrors makes it possible to deduce also for **H-FPs** without **IF** and for some of their properties a quantitative model of equivalent cavity filled with homogeneous medium and with localized mirrors equidistant by a fraction of the length of the **Bg** depending only on its reflection coefficient. This equivalent cavity is used to evaluate the line

width. This model also applies to 2 **Bg-FPs** without **IF** with a double length of the equivalent cavity for the same grating.

Highlights

- Hybrid Fabry-Pérot (**H-FP**) = multilayer mirror + Bragg grating (**Bg**) = ultra-narrow bandpass and wide rejection
- **3D S**-matrix-simulation indispensable at least to determine the boundary layer with the **Bg** even despite little diffraction in the layers, and also for **Bg** having high refractive index step
- Detailed study of the transmission peak, rejection band and manufacturing tolerances of **H-FP**
- Comparison with **Bg-FP** (where both mirrors are **Bg**) and simulation of **H-FP** and **Bg-FP** with fibre between their mirrors
- Deduction of an equivalent model of the **H-FP** and **Bg-FP** explaining quantitatively their line width

Keywords

Narrow bandpass filter, Optical fibre, Integrated Optics, Modal Simulation, S Matrix

1. Introduction

Hybrids Fabry-Pérot (**H-FP**) were introduced in [1] by **1D** numerical simulation. They consist of a multi-layer mirror of all-quarter-wave optical thickness layers located at the end of a Bragg grating (**Bg**) embedded in an optical fibre, for example, so that at the interface, the periods of the grating and the multi-layer are in phase opposition (fig.1a). The interest of **H-FP** presented in [1] is to obtain a bandpass filter a few pm wide in a rejection band several hundred nanometers wide, simultaneously obtaining the advantages of **FP** with 2 Bragg mirrors (**Bg-FP**) and **M**ultilayer fibred **FP** (**M-FP**) without their disadvantages. In [1], phase opposition was obtained by an additional photosensitization

of any distribution, but whose overall intensity was adjusted in the axial direction, at the interface between the multilayer glued onto the cleaved **Bg**. Serial multiple **H-FPs** were also simulated in [1]. Have been simulated in [2] very narrow 2-band **H-FPs** called "bicornes", and in [3], "chirped" **Bg-H-FPs** (with pseudo-periodic **Bg's** whose period varies for example linearly along the optical axis *z*). A **H-FP** with phase opposition adjustment during the multilayer deposition by adjusting the thickness of its boundary layer with the end of the cleaved **Bg** was then experimentally performed with a 100 pm passband [4, 5]. Finally, in [6], a **H-FP** was performed by adjusting the phase opposition by polishing adjusting the millimetre to sub-millimetre length of interleaved fibre (**IF**) between a photo-recorded **Bg** in a cleaved fibre beyond the photo-recording, and a multi-layer mirror deposited at the end of another fibre (the whole being maintained in a ferrule), getting so an **IF-H-FP** with 9 pm passband in a 400 nm rejection band. This amounts to considering in addition a section of fibre interleaved between the multilayer and the **Bg** of figure 1a as in figure 1b.

The **1D** calculations made in [1] were based on certain assumptions:

- Single-mode propagation throughout the **Bg** of the **H-FP** in the direction of propagation z
- In the case of a **Bg** where the core refractive index $n_{co}(z)$ and the optical cladding index $n_{cl}(z)$ vary sinusoidally, sinusoidal variation of the effective index of the fundamental mode $n_{eff}(z)$
- Propagation of a plane wave orthogonal to the layers through the **H-FP** multilayer, with in particular no diffraction

Thus, Bragg gratings were simulated in **1D** using the characteristic matrix method [7, 8] as multilayers having as refractive indices the effective indices of the fundamental mode in each sample of the Bragg grating period.

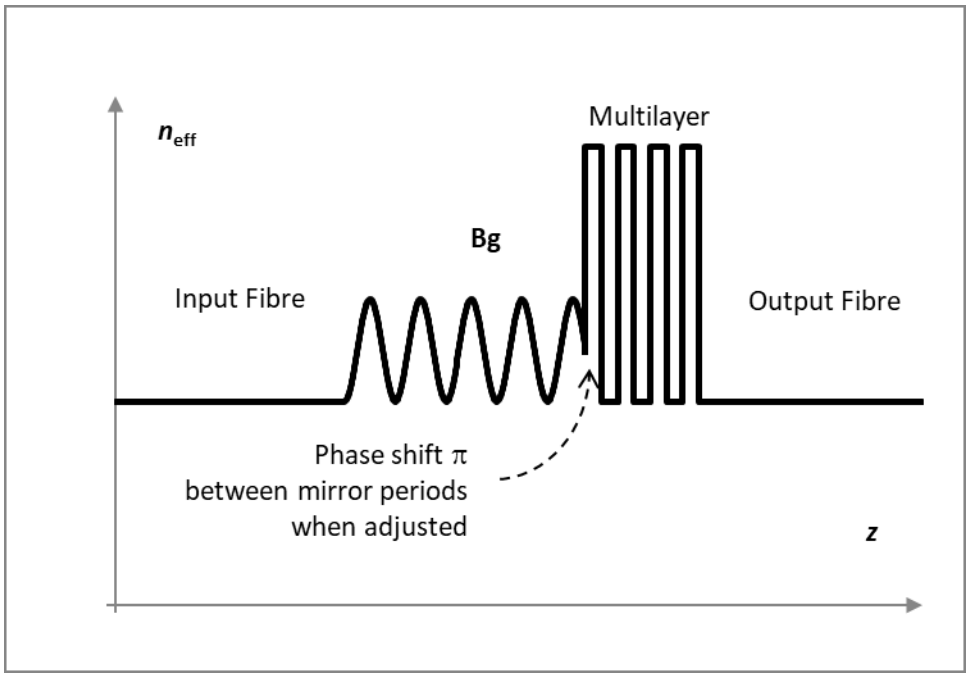

Figure 1.a: Schematic diagram of **H-FP**. Note the phase shift between the **Bg** period and the multilayer mirror period appearing at a certain *z*-position. In the simulations of [1, 2, 3], this position is any, and the phase between the two periods is adjusted by UV photo-refraction applied to the whole **H-FP**. In [4, 5], this position and so the phase, are adjusted by accurately controlling the thickness of the interface layer of the multilayer with the **Bg**. The representation in this diagram is not to scale.

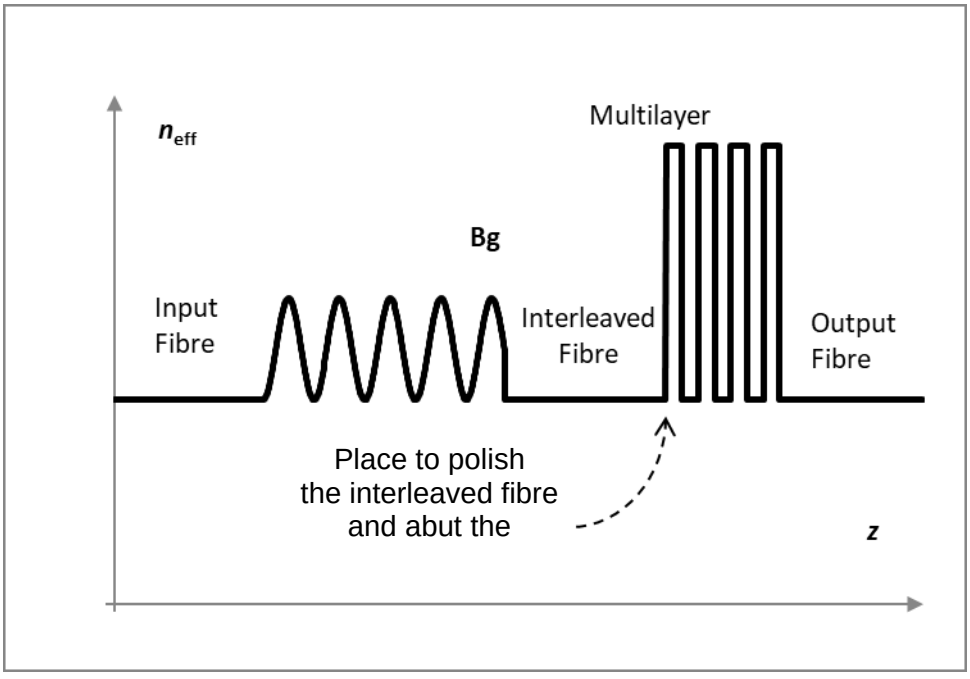

Figure 1.b: Schematic diagram of an **IF-H-FP** constructed in [6]. The **Bg** is photo-written in a fibre with un-photo-written parts remaining besides with interfaces at any period position of the **Bg**. The multilayer is butted against one of those parts. The phase between the period of the **Bg** and this of the multilayer is any. The phase between the periods is then adjusted by several trials of polishing this fibre part and abutting it against the multilayer.

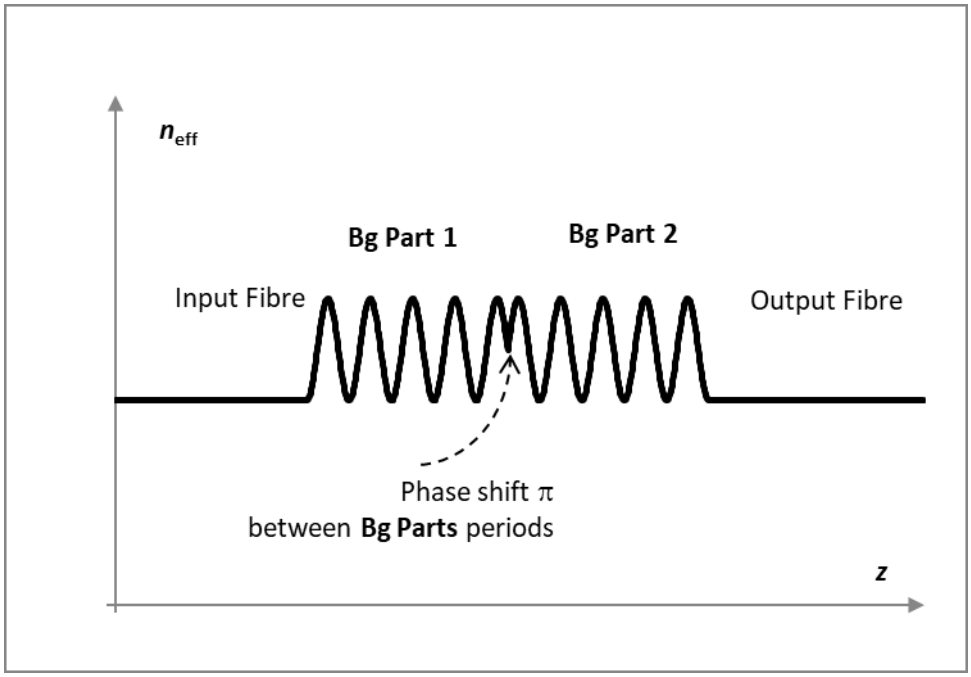

Figure 1.c: Schematic diagram of a **Bg-FP** as constructed in [13]. The phase shift introduced between the periods of the 2 parts of a **Bg** gives them the role of the 2 **Bg** mirrors of a **FP**.

Here, the **H-FP** simulations are taken over with a **3D** calculation method based on the expansion in eigenmodes and calculation of the propagation by **S-matrix**. This method used in [9, 10] is well adapted to the calculation of multilayer filters between fibres and has shown that diffraction is important through a very optically resonant **M-FP** (**M**ultilayer **FP**) between optical fibres with narrow cores. To do this, we use a configuration of guided wave software distributed by Photon Design: Fimmwave for mode calculation, and Fimmprop for propagation calculation by **S-matrix**. Radially about the z-axis, the thin layers of the multilayer mirrors are each considered as a fictitious fibre with a uniform refractive index within the metal limit boundary conditions resulting in guidance. This

boundary is radially located at $\rho = \rho_F$ far enough from the propagation axis for the electromagnetic field to be negligible (ρ is the radius in cylindrical coordinates around the *z* axis).

We are considering fibre optic technology here because it is well known by a broad community of researchers. But the concept of a hybrid **FP** with one mirror with a high refractive index step and the other with a low refractive index step can be extended to integrated optics technologies, which are very diverse. Of course, multilayer mirrors can only be realized at the external interfaces of integrated optics circuits, but it is possible to obtain mirrors with such a high index step as in multilayer mirrors even in the core of integrated optics circuits by using photolithography or etching. Moreover, the intermediate refractive index step range between that of thin films (from 0.1 to a few units) and that of photorefractive **Bg** (from 10^{-6} to 10^{-1} in silica [11]) is accessible in integrated optics by ion implantation [12]. Thus, in integrated optics, it is possible to produce hybrid filters whose mirrors have any index step between 10^{-6} and a few units.

The first purpose is here to verify in which cases the assumptions made in [1] for the **1D** calculation are verified or not. Therefore, the properties of the **H-FPs** will be studied more fully than in [1] by **3D** modal simulation. In [4, 5], only experimental results on a fibred **H-FP** adjusted via the thickness of the interface layer of its multilayer with its **Bg** were presented: the theory and simulation will be extensively developed here. Weak spectral oscillation of the transmission in the rejection band, which had not been described nor interpreted before, are also studied here. We will show that the study of **IF-H-FP** contains information leading to a new quantitative model to interpret the **FP** properties of **H-FP** and **Bg-FP** without **IF**. Here, only single **H-FPs** are studied, and serial multiple **H-FPs** will be presented in another publication.

Bg-FP (figure 1 c) have been constructed by UV irradiation through a mask with a π phase difference between the periods of the 2 parts of the mask [13]. Provided that **Bg-FP** have poor rejection properties (as explained at the end of § 3.1), **FP** applications as bandpass filters are DWDM and sensors and are only industrially available in 2021 in non-fibre form thin film technology where the

bandwidth is at least 100 pm. We will see here quantitatively to what extent hybrid filters not only allow to strongly push back these limits, but also in fibre or integrated optics technology.

2. Theory

This chapter gathers and précises some more or less known elements useful to the readers as **S**-matrix formalism, the notation used for the multilayer and **Bg** inside the grating, the **S**-matrix simulation of **Bg**, and the concept of phase difference between the periods of 2 reflectors.

2.1. Summary reminder on propagation simulation by S matrix

Since the eigenmodes of the fibres are calculated in advance by Fimmwave, Fimmprop simulates propagation by a simple **S**-matrix calculation that is much faster than a direct analytical calculation would have been [8, 9, 10, 14]. In all the calculations made here, we study the system's response to mode 1 injected only as an input into the left access, the left access fibre being identical to the right access fibre having the same number d of modes. If power 1 has been injected in mode 1 on the left, the device response is given by the power coefficients T_{1n} and R_{1n} only, where the matrices **R** and **T** are sub-matrix of the **S**-matrix (modal Reflexion from left to left, and transmission from left to right). These coefficients check:

$$1 = \sum_{n=1}^{d} T_{1n} + \sum_{n=1}^{d} R_{1n} + A + L_C \qquad (\text{Eq. } 1)$$

A represents the absorption losses if not negligible. L_C is calculated by Fimmprop and represents the losses due to the calculation that exist if the number of modes or spatial resolution are insufficient. If $A = L_C = 0$, and if there is no diffraction, for an **H-FP** between fibres in which the only mode 1 is injected on the left, Eq. 1 is reduced to $T_{11} + R_{11} = 1$. For such a filter, the other coefficients T_{1n} and R_{1n} are all the more important as there is diffraction in the multilayer where the beam expanding from the fibres is not guided [9, 10].

2.2. Bg profiles notations & Bg S-matrix simulation

We call everywhere λ_0 the centre wavelength for which the layers of multilayer mirrors are quarter-wavelength layers[1] and it is also chosen as the Bragg wavelength of the gratings. A multilayer mirror between identical **F** fibres is noted **F,[(HL)^{N}H],F** where **H** and **L** are High and low refractive index n_H and n_L quarter-wavelength layers of thickness t_H and t_L, and N is the number of periods.

Photo-refractivity radial profile of fibres and Bg

We consider here the case of the uniform photorefractive radial profile, which is the simplest to calculate. Let $\Delta n(z)$ be the positive photorefractive variation along z of the refractive index. Let n_{co} and n_{cl} be the original fibre indices considered uniform in the core and in the optical cladding, and the indices after UV irradiation $n_{co,i} = n_{co} + \Delta n(z)$ and $n_{cl,i} = n_{cl} + \Delta n(z)$ considered radially uniform. In the case where $\Delta n(z) <<< n_{co} + n_{cl}$, then the single mode approximation can be used, since the fundamental mode is almost the same in the photo-sensitized part as in the non-photo-sensitized part. Modal **3D** simulation will make it possible to verify in which cases $\Delta n(z)$ is low enough for this approximation to be justified.

Photo-refractivity axial profile of Bg's

The **Bg's** obtained experimentally by interference [16] generally have a sinusoidal axial profile according to z, which is correctly sampled with 8 samples per period in the **1D** model [1]. It is also possible to realize step rectangular axial profile gratings by masking the photo-inscription UV beam, or by relative displacement of the fibre to be irradiated with an impulse UV laser.

"Sinusoidal" Bg: We choose to model the period of length Λ with a beginning and an end corresponding to a lack of photosensitization. Then, the core and optical cladding refractive index $n_{co}(z)$ and $n_{cl}(z)$ in the period are periods of sinusoids with minimums at the beginning and the end of the period and with a full amplitude Δn. We have checked that the effective index of the irradiated

[1] $\lambda_0 = 4nt$ for a layer of thickness t and refractive index n

fibre follows also a sinusoidal law $n_{eff}(z)$ with minimums at the beginning and end of the period and full amplitude Δn. The Bragg relationship for the fundamental mode is:

$$\int_{z=0}^{\Lambda} n_{eff}(z)dz = \frac{\lambda_0}{2} \qquad \text{(Eq. 2)}$$

The sinusoidal law $n_{eff}(z)$ in Eq. 2 gives then:

$$\Lambda = \frac{\lambda_0}{2\left(n_{eff} + \frac{\Delta n}{2}\right)} \qquad \text{(Eq. 3)}$$

Fimmwave has functions developed to edit such adiabatic evolution devices according to z (class of "tapers" where it is here the refractive index of the core and the optical cladding that vary slowly with z, and where an optimizing internal algorithm does not necessarily choose $z_{S,j}$ samples of uniform length). This avoids editing each sample of a sinusoidal **Bg** as soon as you want to modify the precision of the sampling, which would be extremely tedious (would require editing each sample and then calculating n_{eff} of its fundamental mode). Here, it is sufficient to enter the sinusoidal functions $n_{co}(z)$ and $n_{cl}(z)$ and specify "Min_Step_Frac" $\triangleq$ *MSF* $\triangleq \Delta z_{Min}/\Lambda$, the parameter representing the minimum fraction of the sample in the period. Fimmprop obtains the exact period Λ of the **Bg** by scanning Λ to obtain a minimum of T_{11} of the **Bg** of the **H-FP** at $\lambda = \lambda_0$. We have carefully verified that the results are identical by introducing these elaborate functions or by introducing the period of the **Bg** sample by sample. This verification was necessary because the exact way in which speed sampling is done by Fimmprop in the tapers is a trade secret that is not disclosed.

“Quarter-wave” Bg: We define this kind of step **Bg** as a grating with 2 samples per period, of different lengths, built quite like a quarter-wavelength multilayer mirror. The first sample of the **Bg** period is the input-output fibre of the **H-FP**. The other sample has its core and optical cladding indices incremented by the same Δn value by photo-refractivity. The thickness of each sample is then:

$$t_{l,h} = \frac{\lambda_0}{4n_{eff_{l,h}}} \qquad \text{(Eq. 4)}$$

where the low and high effective indices of the fundamental modes of the respective 2 samples are involved. The quarter wave **Bg** is convenient to set the phase shift between mirror periods (e.g. by ending the **Bg** with a t_h photo-written **Bg** fibre section on which the first complete **H** layer of t_H thickness is deposed). So, the quarter-wavelength **Bg** leads to quick conclusions on step **Bg's** with simulation, but is rarely manufactured, despite it could be with a mask.

Note that the difference in refractive indices between 2 samples adjacent inside a sinusoidal **Bg** becomes as small as desired by increasing the number of samples, allowing a very fast single mode calculation. Thus, in **3D**, the calculation of sinusoidal **Bg's** in single mode approximation promises to be much faster than the mandatory multimode calculation of step **Bg's** with high Δn. To predict the number of useful modes for simulating step **Bg's**, we will proceed as follows:

- We consider only the fundamental mode in the input and output fibres, as well as in the non-photosensitized part of the **Bg** period, which is identical to these fibres

- By analysing with Fimmprop the device constituted by a single period of the **Bg**, composed of non-photosensitized fibre followed by a joint and with photosensitized fibre, we look for the expression of the mode of the 1st fibre of the period in the base of the modes of the second, i.e. the coefficients T_{1n} of the **S-matrix** of this device, retaining only the highest T_{1n} value modes. This composition of modes in the second fibre then reforms the fundamental mode of the first if it is injected into a subsequent period of the **Bg**, confirming the possibility of single mode simulation in the first fibre of the period. The acceptable limit is confirmed by checking whether for the global balanced hybrid filter, T_{11} is sufficiently close to 1 at λ_0 with respect to the criterion that has been set.

Except for the determination of these limits, most of the properties of **H-FPs** are identical for sinusoidal or step **Bg's**: we will therefore check them only on **H-FP** with sinusoidal **Bg's**, faster to calculate.

2.3. Definition of the phase shift of the Bg and multilayer periods

The period phase definitions for initially setting intuitively the correct phase shift at the interface between the **Bg** period and that of the multilayer mirror are as follows:

- For the **Bg**, we set the phase origin at $z_0 = 0$ where $\Delta n_{\text{eff}}(z) = 0$, and the phase of the period is defined as:

$$\varphi(z) - \varphi(z_0) = 2\pi \frac{\int_{z=z_0}^{z_0+z} \Delta n_{eff}(z)\,dz}{\int_{z=z_0}^{z_0+\Lambda} \Delta n_{eff}(z)\,dz} \equiv (2\pi) \qquad (\text{Eq.5})$$

- Inside the quarter wavelength multilayer mirror, the beam is strongly multimode and bidirectional. The only simple approximation we can try to make before using Fimmprop is to assimilate it as in the **1D** model to a plane wave propagating orthogonally to a stack of layers of refractive indices n_L and n_H. The calculations made with Fimmprop will tell us if this approximation is justified. We set the origin $z_0 = 0$ at the centre of a quarter wavelength layer **L**, and with the period thickness $e_P = e_H + e_L$, the phase of the period is defined as:

$$\varphi(z) - \varphi(z_0) = 2\pi \frac{\int_{z=z_0}^{z_0+z} n(z)\,dz}{\int_{z=z_0}^{z_0+e_P} n(z)\,dz} \equiv (2\pi) \qquad (\text{Eq.6})$$

Thus, we can easily find that for a multilayer mirror, in the direction of increasing z, the phase is $\pi/2$ at the beginning of an **H**-layer of the period starting in the middle of a layer **L**, π in its centre, and $3\pi/2$ at its end.

For the **Bg**, we could find according to intuition that the phase is π in $z = \Lambda/2$ and 2π in Λ. On the other hand, only the integration formula makes it possible to find the less intuitive results[2]:

[2] Only if $n(z)$ was constant over the period (which is not the case!) would we have found $\varphi(z)$-$\varphi(z_0) = 2\pi$ mantissa of (z/Λ) and therefore the phase differences $\pi/2$ instead of the 2 phase differences calculated just above.

$$\begin{cases} \varphi(\Lambda) - \varphi(3\Lambda/4) = \varphi(\Lambda/4) - \varphi(0) = \dfrac{\pi}{2} - 1 \\ \varphi(3\Lambda/4) - \varphi(\Lambda/2) = \varphi(\Lambda/2) - \varphi(\Lambda/4) = \dfrac{\pi}{2} + 1 \end{cases} \qquad \text{(Eq.7)}$$

Both Eq. (5, 6) will be used as first step to find the ideal phase jump between the periods of the **H-FP** reflectors in the **S**-matrix simulation.

3. Choice of H-FPs structures with perfect manufacturing

Concerning the manufacturing tolerances, the periodicity of **Bg** and multi-layer mirrors is sufficiently controlled [16, 17]. The delicate point is the control of the phase shift of their periods at the interfaces, particularly between the two different technologies of layer deposition and **Bg** cleavage or polishing. For a single serial **H-FP**, insufficient control of the thickness of the interface layer with the cleaved or polished **Bg** will result in a spectral shift of the transmission peak, and its subsidence.

The ideal bandpass filter has a narrow bandwidth with step flanks and a wide rejection band with a high rejection ratio. In this chapter, where we are just trying to choose the structures (multilayer formula and **Bg** *z*-profile), the manufacturing is assumed to be perfectly controlled.

Before introducing new material in this chapter, we recall some points introduced in [1]:

- The compactness of the **H-FP** according to *z* is mainly limited by that of the **Bg**.
- Outside the spectral areas where the gratings are reflective, an **H-FP** behaves like the multilayer it contains, i.e. a mirror whose reflection fixes the filter rejection.
- Multilayer mirror's reflection increases and approaches 100% when the number of layers is increased to a certain number determined by the qualities of the materials in terms of absorption.

It is easy to check that the formula for multilayer is not suitable for **Bg** and vice versa (try for example the formula for **Bg** for multilayer with $\Delta n_{eff} = 0$ in layer **L** and $\Delta n_{eff} = n_H - n_L$ in layer **H**: the phase of the period is then constant all along the **L** layer, which is not convenient!).

- The rejection is wider band if the mirror is made with a pair of materials having a high step of refractive index between them, which also has the advantage of a faster deposition of fewer layers.

- In any case, care should be taken that some moisture-sensitive materials must be encapsulated.

3.1. Obtaining balanced H-FPs

It had been demonstrated in [2] that when at centre wavelength λ_0, the **Bg** reflection equals that of the multilayer at λ_0, the **H-FP** is said to be balanced and a single bandwidth filter is obtained centred at the centre wavelength where the transmission is 100% [3].

To obtain a single 100% transmission bandwidth, for a given number of layers of the multilayer mirror, it is therefore necessary to adjust the number of periods of the **Bg** to obtain a balanced **H-FP**, which is observed when its transmission goes back to 100% at λ_0. This was done roughly in [1] by 1D simulation. Here, we make it accurately in **3D S**-matrix simulation. It is important not to make the mistake of optimizing the reflections of the multilayer mirror and Bragg grating separately at λ_0 between 2 input-output fibres. Indeed, this gives a quite different result since the refractive index of one at less of the multilayer materials and that of the fibres are very different from each other. On the other hand, if the index step Δn *of* the quarter-wave **Bg** is fixed, it must be taken into account that the step of refractive index between the layers of the multilayer mirror being fixed at a different value, the values of the reflection coefficients are discrete and therefore cannot be adjusted perfectly. This is all

[3] It had also been demonstrated in [2] that:

- When at centre wavelength λ_0, the reflection of the grating exceeds that of the multilayer, which is spectrally almost invariant, a double bandpass or bicorne filter is obtained, whose bands are centred on both sides from λ_0 to wavelengths where the reflection of the grating equals that of the multilayer.

- When the **Bg** reflection is lower than that of the multilayer at λ_0, we obtain a single bandpass filter centred at λ_0 but with a transmission level that is all the lower the more different these reflections are.

the more critical when Δn is high. So, unless Δn can be adjusted perfectly, the maximum transmission of the **H-FP** is in general slightly less than 1, even if the N_{Per} number of whole periods of the **Bg** is adjusted as best as possible.

H-FP vs Bg-FP comparison

The main difference is that a **H-FP** has a spectrally uniform mirror over a very wide band compared to the main reflection band of its **Bg**. In a **Bg-FP**, **Bg's** have identical secondary reflection peaks at the same wavelengths. So at all these wavelengths, the **Bg-FP** is balanced and has secondary transmission peaks up to $T_{11} = 1$ in addition to the main transmission peak at λ_0. In addition to the narrow reflection band of their **Bg**, this is why **Bg-FPs** have a considerably narrower rejection band than **H-FPs**.

3.2. Setting the phase shift of the multilayer and Bg periods

Provided that the bundle of gratings has been photo-written and then cleaved or polished identically for every fibre by collective manipulations, adjusting this phase shift by adjusting the thickness of the interface layer of the multilayer as only experimentally done in [4, 5] has the advantage of easily allowing mass production by depositing at the end of a bundle composed of many fibres, but its accuracy is limited by that of the deposition technology used. On the other hand, the setting of the phase shift by UV photosensitization at the interface soon simulated in [1], subsequent to manufacturing, is not limited in accuracy, but is less easily suitable for mass processing. Here, we will therefore present the until now unpublished theory and simulations only of adjusting the thickness of the interface layer to evaluate its limits according to those of CVD technology.

Note **F,[(HL)^{N}H,π,Bg],F** or **F,[Bg,π,(HL)^{N}H],F** a simple **H-FP** between fibres **F,** and **F,[Bg,π,Bg],F** a **FP** purely in Bragg gratings noted **Bg-FP**. In each of these **FPs**, the mirror periods are out of phase by π.

- To obtain this phase shift in a **H-FP** with quarter-wave **Bg**, there are an infinite number of ways, but the easiest to program is to put a sample **h** of thickness t_h of the **Bg** (where **h** and t_h

have been defined for the **Bg** in the same way as **H** and t_H for the multilayer) next to a layer **H** of thickness t_H of the multilayer mirror.

- In the case of **H-FP** with a sinusoidal **Bg**, regardless of the termination of the **Bg**, phase optimization can be simulated by scanning with Fimmprop the e_{trim} thickness of the **H** layer adjacent to the **Bg** to obtain a maximum of $T_{11}(\lambda_0)$ for the **H-FP** (an experimenter would control the thickness of the adjacent **H** layer by measuring extremes of the transmission or reflection of the filter during its deposition).

3.3. Shift of a plane wave FP transmission peak in function of e_{trim} variations

λ_v is the wavelength in the vacuum at the top of the transmission peak. We deduce after Eq. A8 that if the equivalent length L_{Eq} of the cavity (filled with uniform refractive index n_{eff}) changes of δL_{Eq}, the wavelength of the considered Airy peak is translated in an inversely proportional way to L_{Eq} of the value:

$$\delta\lambda_v = \frac{\lambda_v}{L_{Eq}}\delta L_{Eq} \qquad \text{(Eq. 8)}$$

The Appendix A model on plane wave **FP** in which the reflection coefficients of the mirrors are real is useful especially for simulating **H-FP** with **IF** where the phase opposition between the periods of the mirrors is determined by adjusting the length of **IF**. For **H-FP** without **IF**, the multilayer mirror has a complex reflection coefficient whose complex exponential parts phase shift can be grouped into the phase φ defined in Eq. A2 and modified according to:

$$\varphi = 2\, n_{eff}\,(2\pi f / c)\, L + 2\, n_H\,(2\pi f / c)\, e'_{trim} \qquad \text{(Eq. 9)}$$

where e'_{trim} is a fictive suitable thickness of material **H** to express the phase shift between the mirrors, and remaining less than around λ_0. If the thickness e_{trim} of the layer **H** boundary with the **Bg** varies, we have $\delta e'_{trim} = \delta e_{trim}$. After Appendix A, we arrive to:

$$\Leftrightarrow \delta\lambda_V = \frac{n_H \lambda_V}{n_{eff} L_{Eq} + n_H e'_{trim}} \delta e_{trim} \simeq \frac{n_H \lambda_V}{n_{eff} L_{Eq}} \delta e_{trim} \qquad \text{(Eq. 10)}$$

The last approximation is valid because $e_{trim} < \lambda_0$ and the results of § 4.6.3 will show that for any **H-FP**, $L_{eq} >> \lambda_0$.

3.4. Secondary transmission peaks of the H-FP

The existence of a single peak transmitting almost 100% in a narrow band for the single **H-FP** is due to the uniqueness and spectral narrowness of the band where the **H-FP** is balanced. However, secondary transmission peaks studied here for the first time may occur:

- Since at wavelengths other than λ_0, the multilayer keeps an approximately uniform reflection and much higher than that of the quasi-zero **Bg**, even for the much higher secondary reflection peaks of the **Bg**, the **H-FP** is very unbalanced. So, even with the right period phase shift, its corresponding secondary transmission peaks are therefore necessarily very low.

- Another source of low resonances outside the **Bg** reflection band could be the low dioptre between a feed fibre $n_{co,cl}$ and the **Bg** fibre, which outside its reflection band is a fibre of average index $n_{co,cl} + \Delta n/2$.

- A conventional **FP** has spectrally uniform, infinitely thin mirrors, separated by a well-defined length L, and therefore 100% transmission Airy peaks separated by $f = c / (2n_{eff} L)$. This is not the case here because the **Bg** has a few mm to a few cm lengths, and is spectrally selective.

Only numerical simulation will tell us whether such small secondary peaks have a significant amplitude anyway, and what are their spectral properties. For a first fast reading of the whole paper, we signal optional skip reading the chapters dealing with those simulations (4.5.1; 4.5.2; 4.6.2).

4. Simulation results

For the first time, **3D** simulations of hybrid filters are presented here. They will be used mainly to check the **1D** calculation on the main transmission peak of the hybrids, precise the interface layer thickness accuracy exigence, and also to simulate their unpublished secondary transmission peaks.

4.1. Simulation parameters and calculation convergence criteria

The calculations are all the more accurate when ρ_F is sufficient and the "precision parameters" are high, which are: the spatial resolution, the number N_{Mod} of modes in each fibre, and the minimal sample length in the **Bg** period. Nevertheless, quick and sufficiently accurate calculations are obtained for the lowest possible values of these parameters. The criteria used to ensure the accuracy of the calculations will not be recalled each time, but the methods generally used to set these parameters are among the following:

- Convergence of the system **S-matrix** according to the value of these parameters. Most often, only mode 1 (fundamental mode of the input fibre) is injected, and it is sufficient to check the convergence of T_{11} (λ_0)

- Verification of the existence of $L_C(z)$ losses due to calculations made by Fimmprop. The possible occurrence of calculation losses from a specific *z*-position in a device helps to find its origin.

- Convergence of the modal composition of the beam into one or more *z*-positions in the device

- These criteria must be applied to the complete device to be studied, but a preparatory work allowing a first evaluation of the precision parameters is for example to simply examine the injection of a mode of a fibre operating in the device into a neighbour fibre operating in the device.

Number of modes N_{Mod}

The modes are such that their complex E_z component is $E_z(\rho,\theta) = E_z(\rho)\, e^{im\theta}$. Their real E_z component is then described by the m azimuthal and p polarization integer orders:

$$\begin{cases} \text{For modes with order } p = 1 \rightarrow E_z(\rho,\theta) = E_z(\rho)\sin(m\theta) \\ \text{For modes with order } p = 2 \rightarrow E_z(\rho,\theta) = E_z(\rho)\cos(m\theta) \end{cases} \quad \text{(Eq. 11)}$$

If only a mode with $m = m_0$ and $p = p_0$ is injected into the input fibre, throughout the filter, it will then not be useful to consider modes other than m_0, p_0 modes through all the device, which considerably speeds up the calculations (the integrals of overlap between modes of neighbouring fibres and of different orders m or p would be zero, as would the matrices **S** of joint between these fibres).

In this publication, the power injected into the input fibre is always the fundamental mode (mode with highest n_{eff}) in polarization $p = 1$, and with $m = 1$. Throughout the filter, it is therefore useless to consider in each fibre modes other than those with $m = p = 1$. The modes following the fundamental mode are numbered by decreasing n_{eff}, and have increasingly higher radial spatial frequencies. In each fibre, the accuracy of the beam expansion therefore increases with the number of modes. For a given radial resolution, the number of useful modes is therefore limited, because modes with a too high spatial frequency are calculated inaccurately. To check the validity of the modes of a fibre that must form an orthonormal base, Fimmwave tests their orthogonality. Number of useful modes:

- <u>In access fibres:</u> One mode is sufficient if only the transmission coefficients T_{11} and reflection coefficients R_{11} of the fundamental mode between the access fibres have to be calculated. This is always the case at λ_0 for balanced **H-FP** that do not have diffraction to be evaluated and into which only the fundamental mode of the input fibre is injected.

- <u>In multilayers:</u> the modes in the uniform fictitious fibres simulating their layers are very different from the fundamental mode of the access fibres: therefore, a very multimodal calculation is here mandatory.

- <u>In the **Bg**</u>: The single mode approximation is all the better as:

- the photorefractive step modulation of the refractive index remains low in front of the refractive index of the core of the fibre in which the **Bg** has been photo-written (chosen here identical to the access fibres)

- the variation according to z of the photo-refractivity is adiabatic (e. g. sinusoidal profile more adiabatic than step profile).

We consider the wavelength λ_0 = 1.55 μm throughout the simulations. For greater numerical clarity in the spectra, the wavelength is noted $\lambda = \lambda_0 + \delta\lambda$, and the spectra are all displayed according to $\delta\lambda$. The input and output fibres of all filters are of the SMF28 single mode standard for telecommunications at 1.55 μm (step radial profile fibre with core radius 4.1μm, n_{co} = 1.449, n_{cl} = 1.444; simulated optical cladding extending only to ρ_F where the field is almost null). Multilayer mirrors are always chosen here made with high index **H** in Si and low index **L** in SiO_2 layers of quarter wavelength thickness at $\lambda_{0,}$ and refractive indices of 3.48 and 1.444 respectively. These mirrors, whose layers have a high contrast index (≃2), when between two SMF28 fibres, have with only 7 layers (N = 3) a reflection R_{11} = 99.65% between fibres. We will keep N = 3 everywhere, which allows us to obtain very resonant **H-FPs.**

4.2. Verification of the assumptions of the 1D calculation

The precision parameters that allow to converge better than 0.5% on the value of $T_{11}(\lambda_0)$ are in all cases:

- $\rho_F \geq 20$ μm. The results will show that the structures studied have almost no diffraction: also the beam extends little radially, and it is logical to be able to use ρ_F clearly weaker than in [9, 10] where the highly resonant multilayer **M-FPs** between SMF28 fibres studied introduce a lot of diffraction and where ρ_F had to be fixed at 40 μm.

- 49 modes in the layers of multi-layer mirrors

- A radial resolution N_{Res} = 1000 for Fimmwave's cylindrical finite difference mode solver (FDM) used with electric wall boundary conditions (perfect metal).

- A $\lambda_0/10$ spatial resolution of the modes.

For each $z_{S,i}$ sample of the sinusoidal **Bg**, the calculation by Fimmwave shows that $n_{eff}(z)$ strictly follows a sinusoidal law, as was only supposed in [1]. With a photorefractive amplitude $\Delta n = 2\ 10^{-3}$ and for $N = 3$, the **H-FP** with rectangular **Bg** is balanced with 2544 periods of the **Bg**, while the **H-FP** with sinusoidal **Bg** is balanced with 2679 periods of the **Bg** each with length $\Lambda = 0.5355622$ μm calculated with $MSF = 0.025$. The spectra $T_{11}(\delta\lambda)$ of both **H-FPs** are represented in figure 2 in the 2 cases where their **Bg** are considered multimode (9 modes) or singlemode (1 mode). The following deductions are made:

For the **H-FP** with quarter-wave **Bg**, the single-mode approximation in the **Bg** is not justified near resonance. In particular, the single mode 1D calculation made in [1] is only a rough approximation to the nearest 15% (estimated in figure 2 from the deviation of $T_{11}(\delta\lambda)$ calculated with 1 or 9 modes[4]). It has been verified that the convergence of calculations allowing to have for the **H-FP** $T_{11} > 99\%$ requires 9 modes in the photosensitized fibre of the **Bg** period. In the expansion of the fundamental mode of the un-irradiated fibre based on the modes of the irradiated fibre, the 1st power coefficient is 0.999999992, the next 8 are in the range $[2\ 10^{-9},\ 10^{-7}]$, and the next smaller ones, are neglected. Contrary to what their low value would suggest, the coefficients of the 8 modes following the fundamental are not negligible in the calculation for the **H-FP** of T_{11} at $\delta\lambda = 0$: on the one hand because the **Bg** presents a large number of periods, and more especially because it is one of the mirrors of a resonant **H-FP**. On the scale of figure 2, we see that 9 modes are sufficient because the maximum of $T_{11}(\delta\lambda)$ goes up to 99.13%. On the other hand, since $T_{11}(\delta\lambda)$ approaches 100% better than 1% (most part of which is due to the discrete nature of the **H-FP** balancing with the adjustment of the number of periods in the **Bg**), and since the shift of the maximum of $T_{11}(\delta\lambda)$ from $\delta\lambda = 0$ is only -1.25 fm, the diffraction (accurately explained in [9, 10]) is negligible. Figure 2 shows that whereas the

[4] Be careful that the uninformed user satisfied with a single mode calculation in the **Bg** could have confused this deviation with diffraction in the multilayer!

single mode simulation gives $T_{11}(\delta\lambda = 0) = 87.68\%$, a resonance value 11.4% lower than that obtained by the multimode simulation, the difference is only significant near the **H-FP** resonance wavelength, which is the most important place to characterize a bandpass filter. For calculations outside the resonance, the single mode simulation is still correct.

For the **H-FP** with sinusoidal grating and a period Λ simulated with $MSF = 0.025$, the single-mode approximation is perfectly justified in the **Bg**, since $T_{11}(\delta\lambda)$ rises to 99.54% with 1 mode[5], and since the maximum transmission is precisely for $\delta\lambda = 0$. The transmission peak, which has a FWHM 12.84 pm is nearly 3 times wider than that of the **H-FP** with quarter-wavelength **Bg** (Fig. 2). The simulations have been done after setting e_{trim} to the right value as explained in next chapter.

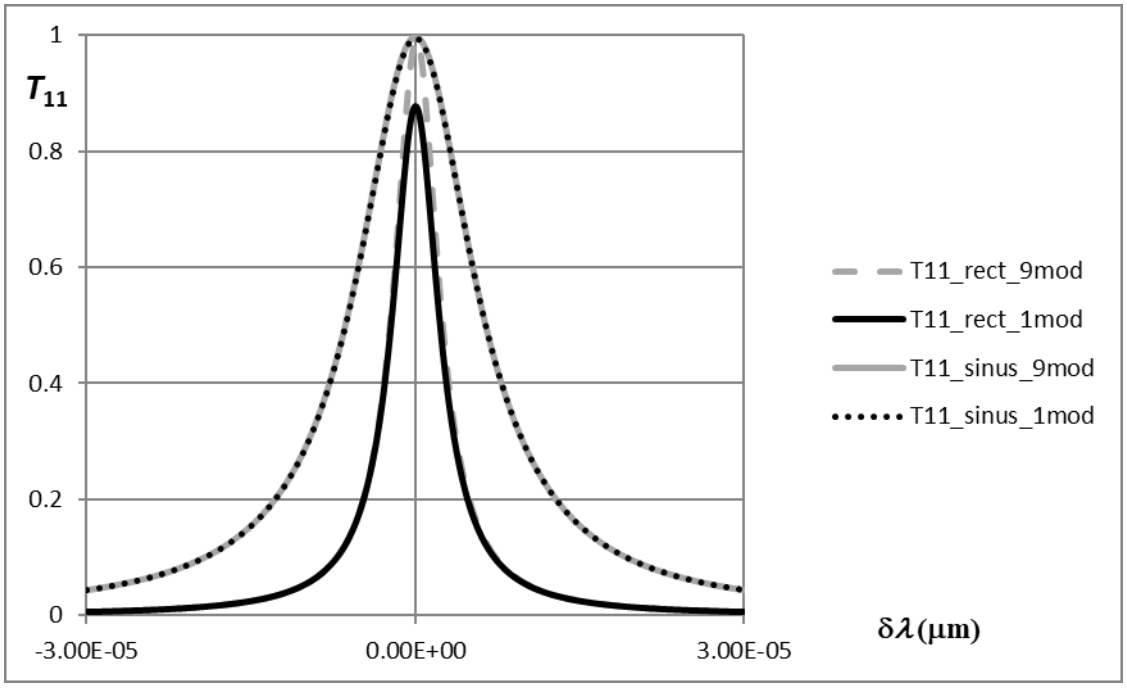

Figure 2: T_{11} ($\delta\lambda$) for single **H-FPs** with quarter-wave rectangular **Bg** profile, or sinusoidal **Bg**, with 1 or 9 modes taken into account in the **Bg**. The curve T11_sinus_9mod is masked by the curve T11_sinus_1mod on which it is perfectly superimposed. Spectral resolution 257 points.

Table 1 shows some properties of balanced **H-FP** with sinusoidal **Bg** as a function of N, which determines the multilayer and therefore also the reflection coefficient $R_{Bg}(\lambda_0)$ of the **Bg** alone between

[5] the single mode calculation at λ_0 gives $R_{11} = 2.74\ 10^{-8}$ and $L_C = 4.59\ 10^{-3}$; whereas the 9 mode calculation gives $T_{11} = 99.66\%$, $\Sigma\{T_{1n}$ other than $T_{11}\} = 4.23\ 10^{-5}$; $\Sigma\{R_{1n}\} = 3.19\ 10^{-3}$; $L_C = 6.82\ 10^{-4}$

fibres. In Table 1, these properties are represented for only one value of the photo-refractivity amplitude Δn of the sinusoidal **Bg**, as simulations show that N_{Per} and $\Delta\lambda$ (FWHM of the transmission peak) are respectively almost inversely proportional and proportional to Δn. According to Eq. 3 or to a Fimmprop scanner calculation described in 2.2, the **Bg** period decreases slightly with Δn. Both ways of calculation give almost the same results[6], and the result of Fimmprop is kept for later calculations by Fimmprop.

Table 1: For a balanced H-FP with a sinusoidal Bg and $\Delta n = 2\ 10^{-3}$, as a function of N of the multilayer: $R_{Bg}(\lambda_0)$ between fibres, N_{Per} and $\Delta\lambda$

N	1	2	3
$R_{Bg}(\lambda_0)$	0.668	0.933	0.988[7]
N_{Per}	1059	1870	2679
$\Delta\lambda$ (pm)	550.3	76.76	12.86

Let **H-FP1** be the single balanced multilayer **H-FP** with $N = 3$ in Si/SiO_2, and **Bg** sinusoidal with $\Delta n = 2\ 10^{-3}$. For the balanced filter **H-FP2** identical to **H-FP1** without $\Delta n = 2\ 10^{-6}$, and optimized e_{trim}, the calculation still gives good results with $T_{11,max} = 0.997$ and FWHM = 13.3 fm, (so about 12.86 fm, which would correspond to an exact proportionality to Δn in comparison with $\Delta n = 2\ 10^{-3}$). In the following, we will no longer consider hybrids of this **FP** fineness for Δn less than $2\ 10^{-6}$, which almost corresponds to the experimental limit of realization of **Bg**, and already allows FWHM as narrow as about 15 fm.

[6] for $\Delta n = 2\ 10^{-3}$, respectively.$\Lambda = 0.5355627$ μm and $\Lambda = 0.5355622$ μm with the precision necessary for a bandpass centring at λ_0

[7] The reasons why this value is lightly different from the 0.9965 value of the multilayer reflection between fibres are explained in Chapter 3.1.

4.3. Adjusting the phase shift between the period of the sinusoidal Bg and that of the multilayer mirror

The **H-FP1** simulation by **S-matrix** shows that:

- The phase shift between multilayer and **Bg** has been obtained for the ideal thickness e_{trim} = 0.2507736μm. Let us check whether the order of magnitude found for e_{trim} corresponds to the simplified model in §2.3. **H-FP1** consists of a **Bg** composed of an integer number of periods as defined in Eq. 3, followed by a multilayer. The phase of the period of the **Bg** at the interface is therefore 0 according to Eq. 5. The phase of the period of the multilayer must therefore be π at the interface, i.e. the interface must be at the centre of a quarter-wave **H** layer according to Eq.6. Experimentally, it is easier to deposit a slightly thicker layer $[(0.5 + 2q)\ e_H]$ where $q \in \mathbb{N}$, which gives very similar spectral characteristics of the multilayer mirror. Since for q =1 Fimmprop gives an optimal value $e_{trim} \simeq 2.25\ e_H \neq 2.5\ e_H$, this shows that the simplified model of §2.3 is not justified. It just helps to explain the concept of phase jump between periods of **Bg** and multilayer, and the bi-directional multi-mode calculation in the multilayer done by **S-matrix** is indispensable to obtain quantitatively accurate results for the value of e_{trim}. So not all the hypotheses of the **1D** calculation are verified: in particular, the multimode calculation of the unguided beam in the multilayer is indispensable to find the right e_{trim} value (the simulations of 4.2 for the **H-FPs** gave a good result in some cases with a single mode calculation in the **Bg**, only because we had soon injected the right e_{trim} value calculated by **S-matrix** into the calculation).

- As experimentally, the deposition of quarter-wavelength layers' stacks is done by measuring extremes of the reflection or transmission of the filter during deposition, we also simulated the deposition of the boundary **H**-layer at the end of the **Bg**. So, we verified

that the optimal e_{trim} value found for the overall filter gives a reflection minimum for the filter consisting only of the grating and an **H**-layer between fibres[8].

- As shown in figure 3, an error δe_{trim} from 0 to about 5 nm on the thickness e_{trim} of the **H** layer adjacent to the **Bg** has almost no effect on the maximum value $T_{11,max}$ of T_{11} ($\delta\lambda$) for **H-FP1**. It has been checked also:

    - That for $\delta e_{trim} \leq$ 5nm, there is almost no broadening of the FWHM $\Delta\lambda$ of the transmission peak.

    - That the curve $T_{11,max}$ (δe_{trim}) of figure 3 stays almost unchanged for any Δn decreasing until $\Delta n = 2\ 10^{-6}$ corresponding to **H-FP2**.

- The simulations show that the top of the transmission peak moves linearly in function of δe_{trim} as predicted by Eq. 10 with $\delta\ \lambda_{Max}\ /\delta e_{trim}$ = +21.09 pm/nm (this numerical value will be compared with these given by Eq. 10 only after knowing L_{Eq} established in § 4.6.3). By keeping N = 3, the simulations show that for R thus fixed, $\delta\ \lambda_{Max}\ /\delta e_{trim}$ is also inversely proportional to Δn, which will be explained in 4.6.4. So, as FWHM $\propto \Delta n$, this shows that the ratio $[\delta\ \lambda_{Max}\ /\delta e_{trim}]$/FWHM is independent of Δn.

- The optical control of the deposit cannot be better than an atomic interlayer distance, i.e. $d_C = (3^{1/2}/4)\ a$ = 0.235 nm for the two closest planes of crystalline silicon with mesh parameter a = 0.543 nm and a thickness of the same order for silica glass. The use of deposition to the atomic layer accuracy alone therefore leads at best to the accuracy of $\delta\lambda_{max}$/FWHM = 38.3%.

- So, the experimenter will have to use all his know-how to adjust the optical thickness of the layers. For example, by using sophisticated optical control during the deposition, and technologies such as ion beam assistance [18], which makes it possible to slightly modify

[8] The minimum reflection thickness found for 0.25070703 μm coincides to e_{trim} to the nearest relative $3\ 10^{-4}$

the density of the material and thus globally the "mesh optical thickness". Other simple approaches that do not allow simultaneous filter production can be used to precisely compensate for the phase shift afterwards: sorting after series production, or additional UV photosensitisation near the interface area as simulated in [1], which can be made as precise as necessary by attenuating the UV beam.

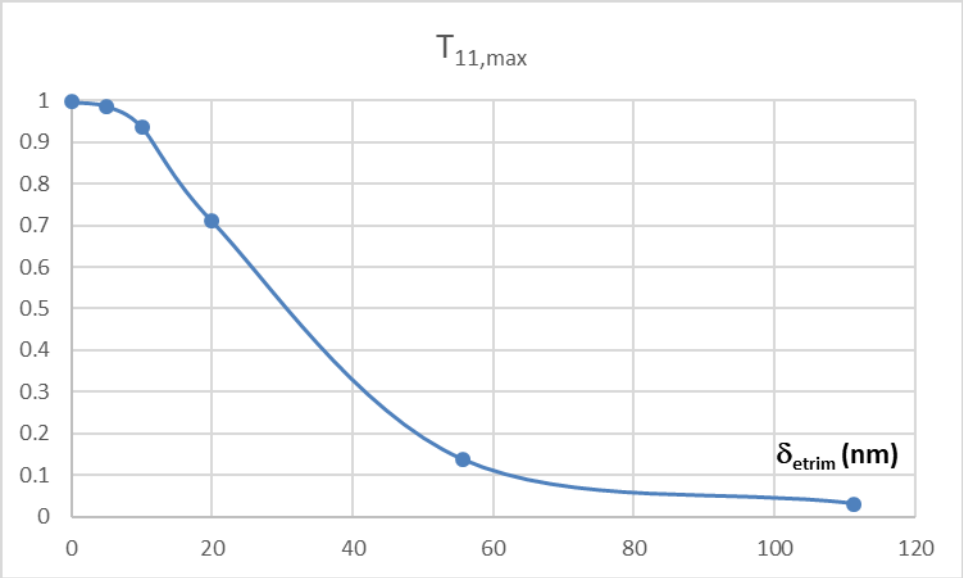

Figure 3: For **H-FP1**, $T_{11,max}$ in function of δe_{trim}.

4.4. Absorption losses

M-FP's have an optically resonant layer between their 2 mirrors, which is responsible for absorption losses effects that can be important [9]. On the other hand, the phase opposition between the periods of the 2 mirrors of a **H-FP** does not require a resonant layer between them: since absorption exists only in the mirrors, low absorption losses effects are expected. We consider losses of 0.15 dB/km typical of telecommunication fibres. In Table 2, we consider typical losses of ordinary to optimal quality layers (from $k = 10^{-4}$ to $k = 10^{-6}$ where k is the imaginary part of their refractive index). It appears in table 2 that the effect of absorption is negligible with good quality layers, very low with the lowest quality layers, and a little bit worse for the narrower

passbands[9]. Furthermore, we observed that the transmission peak in the presence of losses is neither shifted nor asymmetrical with respect to its peak apex. Losses by absorption will therefore no longer be considered here for **H-FP's**. In comparison, in addition to diffraction losses, the absorption losses are the prohibitive element to realize **M-FP** with narrower bandwidth than 100 pm. For **M-FPs**, absorption losses do not only occur in the mirrors as for **H-FPs**, but especially in the layer between these mirrors, which is a multiple layer of 2**H** or 2**L**, and losses are therefore exacerbated in such an optically resonant layer.

Table 2: Losses effects

k	$T_{11,max}$(H-FP1)	$T_{11,max}$(H-FP2)
10^{-4} *	0.97117	0.92344
10^{-5} *	0.99284	0.98816
10^{-6} *	0.99504	0.99500
0 *	0.99529	0.99576
0 **	0.99543	0.99717

* With 0.15 dB/km losses in fibres

** Without losses in fibres

4.5. Rejection and secondary transmission peaks

We have verified that the spectra of the simple **H-FPs** with rectangular quarter-wavelength profile **Bg** verify properties similar to those shown below for the **H-FP1** filter with sinusoidal **Bg** profile. As already noted in § 4.2, multimode simulation in the high index part of a rectangular profile **Bg** is essential mainly at the top of its main transmission peak. We have verified that apart from this peak, for the **H-FP** with rectangular quarter-wavelength profile **Bg** presented in § 4.2, a 9-mode calculation is much longer, but only makes a relative change of less than 4.5 per thousand (reaching the top of the largest secondary transmission peak). Therefore, for **H-FP** to **Bg** with

[9] Without absorption losses in the multilayer, the transmission of both filters appears to be excellent. It is surprising at first sight that the results are there very slightly better for **H-FP2**. But in fact, we are entering an area where computational accuracy should be pushed to the maximum, and this is not significant (as the results are soon excellent for both filters, spending too much time on it is not worth it here).

rectangular profile, the simulation can be single mode in the **Bg**, except for the main transmission peak.

So, the rejection is carefully studied below for the **H-FP1** filter. In figure 4.a, a very wide rejection band (width 0.7 μm with $T_{11} < 0.027$) appears around the transmission peak of **H-FP1**. This band is asymmetrical and has a much better rejection in some areas. In particular, a "super-rejection" band of 1.4445 nm width with $T_{11} < 0.005$ appears (fig. 4.b). The super-rejection band corresponds substantially to the main reflection band of the **Bg** of **H-FP1** that we call **R_Bg Band** (fig. 4.b). In this band, the reflections of the 2 mirrors of the **H-FP** are substantially equal, uniform and close to 1, and their individual transmissions are $T_1 = T_2 \simeq 1.2\ 10^{-2}$ near $\delta\lambda = 0$ (corresponds substantially to the average T_{11} of **H-FP1** outside the **R_Bg Band** on Figure 4.b, where we verified that except the small spectral oscillations of its T_{11} described later, the **H-FP** is strictly equivalent to the multilayer mirror alone). Therefore, according to Appendix A, the minimum transmission that this **FP** can achieve is $T_{min} = T_1^2/4 \simeq 1.44\ 10^{-4}$, which explains well the existence of this super-rejection band if the minimum of T_{11} is close enough of this value. Figure 4.b shows that the minimum $7.1\ 10^{-4}$ of T_{11} achieved for **H-FP1** is intermediate between T_1 and T_{min}. The fact that T_{min} is not reached simply means that the FSR (Free Spectral Range) of **H-FP1** is too much wider than the **R_Bg Band**, which will be demonstrated quantitatively in § 4.6.3 by finding this FSR.

Apart from the **R_Bg Band**, we analyse the **H-FP1** transmission in reference to 2 other bands describing the reflection of the **Bg**: the one called **O_Bg Band** where the **Bg** reflection oscillates with still significant reflection values as in Figure 4.b, and this located outside the **O_Bg Band** where the reflection of the **P**assing **Bg** is almost zero and flat, called **P_Bg Band** (the **Bg** reflection peaks have there $R_{11} < 1.1\ 10^{-4}$).

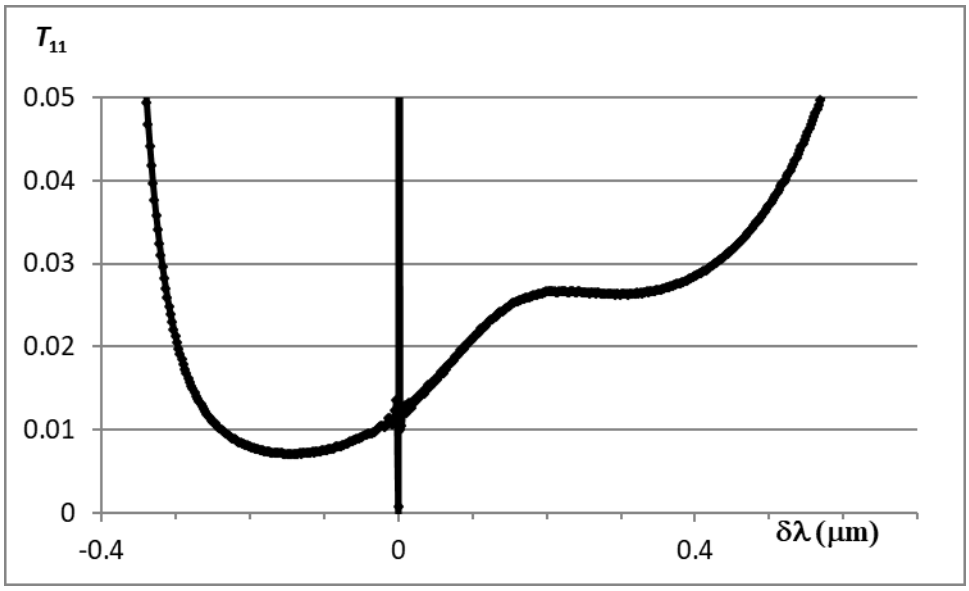

555 **Figure 4.a**: T_{11} ($\delta\lambda$) on the entire **H-FP1** rejection band (transmission peak zone zoomed in fig. 4.b). Spectral resolution 513 points.

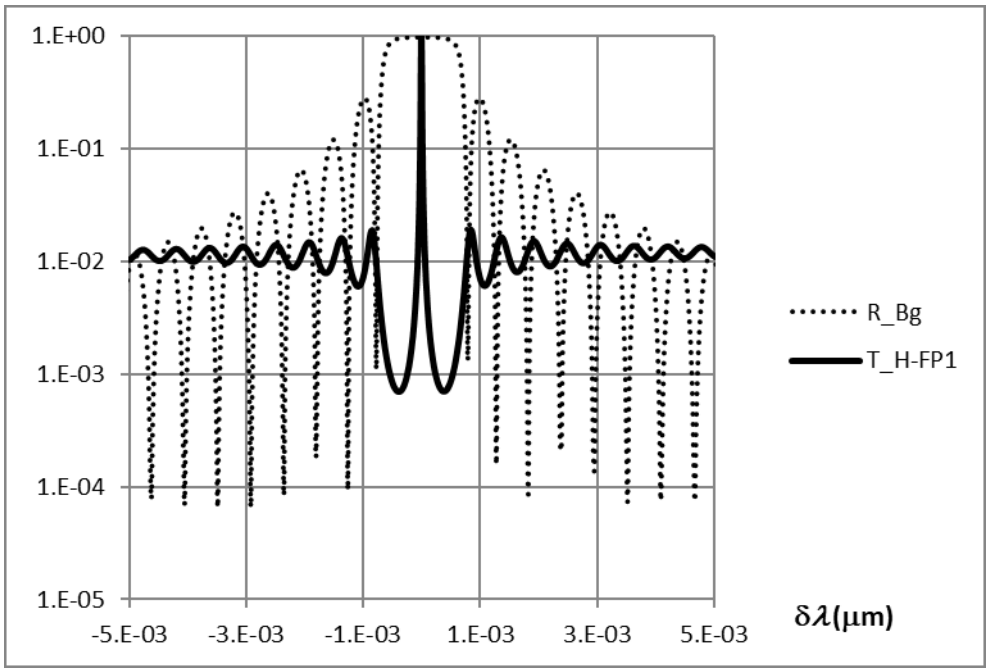

Figure 4.b: T_{11} ($\delta\lambda$) for **H-FP1** and R_{Bg} = 1- T_{11} ($\delta\lambda$) of the included **Bg.** For **H-FP1**, the main transmission peak reaches T_{11} = 0.9955≃ 100%. The most intense secondary peaks are closest to $\delta\lambda$ = 0 and have an amplitude +/- 0.78% of the average rejection T_{11} = 1.2 10^{-2} around and near the super-

rejection band. The main reflection peak of the **Bg** corresponds well to the super-rejection of **H-FP1** and it is centred on the main transmission peak of **H-FP1**.

4.5.1. Transmission of H-FP1 in the P_Bg Band

The simulation in Figure 5 is small part of this band where the $T_{11}(\delta\lambda)$ small peaks of **H-FP1** are closely spaced. It shows very evenly spaced **H-FP1** transmission peaks. We verified that the positions of these peaks do not correspond to the secondary reflection peaks of the **Bg**, which fall rather in anti-phase in the band of the figure, proving that there is no correlation. On the other hand, the positions of these secondary peaks correspond perfectly to a Fabry-Pérot effect between 2 mirrors spaced the length of the **Bg** [10]. We interpret it as one of the contingencies provided for in § 3.4 as the **FP** formed by:

- between the reflectors, the **Bg** considered in the **P_Bg Band** as a homogeneous medium with an average refractive index $n_{eff} + \Delta n/2$ where n_{eff} is the effective index of the fundamental mode of the non-photosensitized fibre.
- as reflectors, the multilayer mirror, and the dioptre of step of refractive index $\Delta n/2$ between this homogeneous medium and that of the input or output fibre considered as another homogeneous medium of index n_{eff}.

[10] The peaks in figure 5 are at frequencies f_1 = 1.81665116 10^{14} Hz; f_2 = 1.81593161 10^{14}; f_3 = 1.81521208 10^{14} giving $FSR_1 = f_1 - f_2$ = 7.19551 10^{10} Hz and $FSR_2 = f_2 - f_3$ = 7.19531 10^{10} Hz. These FSRs have a relative variation of only 2.78 10^{-5}. The corresponding L_{EQ} length = c / (2 n_{eff} FSR) is 1.439944 mm, identical to L_{BG} = 1.434771mm with $\delta L/L$ = 0.33% and $f = c/(2nL) \Rightarrow \delta f/f = \delta L/L$. It was calculated with n_{eff} = 1.446869, the average effective index of the fundamental mode in the **Bg** calculated according to Fimmwave, and for FSR the average of the 2 differences between the peaks above. For the calculation of the average n_{eff}, we start from n_{eff} calculated by Fimmwave for SMF28 at $\delta\lambda$ = 0.101 µm, i.e. in the middle of the scanning range of figure 5, then add Δn photorefractive/2. For $\Delta n = 2\ 10^{-3}$ it comes average n_{eff} = 1.446869. Very similar results are obtained everywhere else in the **P_Bg band**.

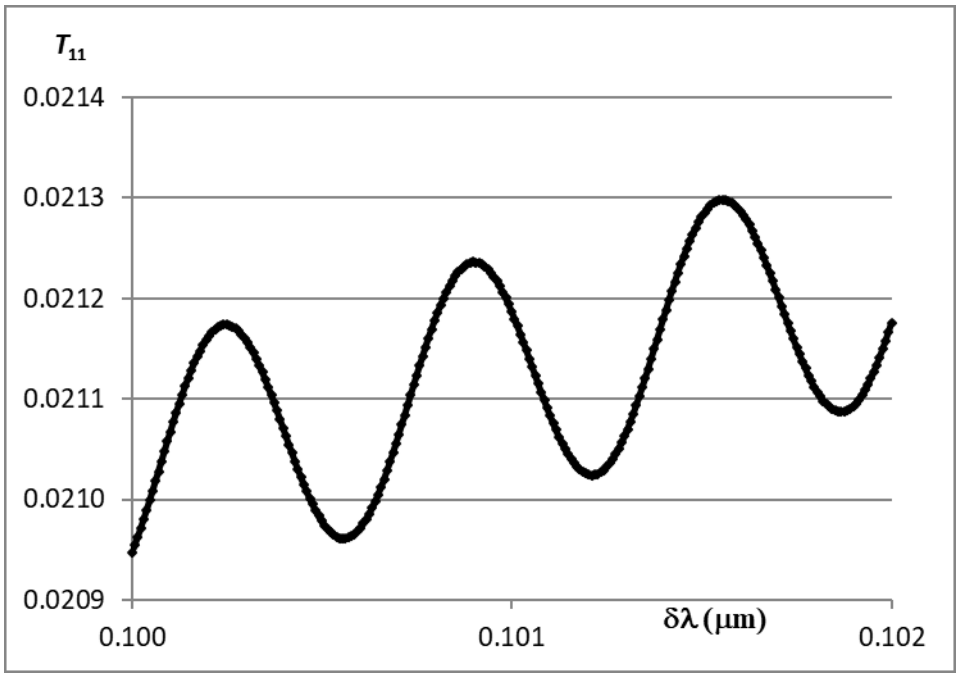

Figure 5: T_{11} ($\delta\lambda$) for the **H-FP1** filter showing some secondary transmission peaks of **H-FP1** in a rejection area of the **P_Bg band** very far from the main transmission peak. The peaks oscillate +/- 0.01% around the average transmission of 2.1% (with an increasing slope as also visible in Figure 4a). Spectral resolution 257 points.

On the frequency point of view, the agreement is perfect to within 0.33% to consider that the oscillations of T_{11} for the **H-FP1** filter in the **P_Bg band** correspond well to an equivalent **FP** of length L_{Bg} (see note 10 again). According to Eq. A5 and A6, the peak-to-peak amplitude of the oscillations should be $T_1 \times 4 \times r_2$. In Table 3, the amplitude of the oscillations have been corrected for the slope shown in Figure 5 at $\delta\lambda \simeq 0.1$ μm. Table 3 shows the interpretations of the amplitude of these oscillations according to 2 ways of calculating r_2. The calculation of r_2 for a $\Delta n/2$ step of refractive index dioptre gives worse results than the calculation of r_2 made by Fimmprop, corresponding to the reflection of the entire **Bg** between an input fibre and the output fibre, for which the match is good for $\delta\lambda$ corresponding to a flat average rejection (table 3 and fig 4.a). For $\delta\lambda$ =0.1 μm, corresponding to a significant slope of the rejection in fig 4.a, only the order of magnitude is quite good in table 3, and the inexact value comes presumably from the slope and the approximate origin of equations A5 & A6.

Table 3: Oscillations of T_{11} for **H-FP1** in three $\delta\lambda$ places of the **P_Bg band**			
$\delta\lambda$ (μm)	$\simeq 0.1$	$\simeq 0.2$	$\simeq 0.3$
T_1	2.11E-02	2.66E-02	2.63E-02
Oscillations amplitude (Fimmprop)	2.12E-04	1.63E-04	1.21E-04
$T_1 \times 4r_2$ (a)	2.91E-05	3.67E-05	3.63E-05
$T_1 \times 4r_2$ (b)	5.22E-05	1.78E-04	3.83E-04

(a) r_2 calculated for a $\Delta n/2$ step of refractive index dioptre located at the fibre-to-**Bg**

(b) r_2 calculated by Fimmprop for the reflection of the **Bg** between SMF28 fibres

595 **4.5.2.Transmission of H-FP1 in the O_Bg Band**

The situation in this band is well represented in figure 4.b, which represents the closest part of this band to the **R_Bg Band**. Secondary transmission peaks spaced at the same order of magnitude as in **P_Bg Band** are observed, but with some notable differences: these peaks are not regularly spaced in frequency (Table 4 corresponding to the peaks in figure 4.b), but closer to each other and more intense 600 when they are closer to the **R_Bg Band**. In figure 4.b, it is clear that these peaks do not correspond either with the secondary reflection peaks of the **Bg**. We suggest that the increase in the intensity of these peaks is however related to the increase in the intensity of the **Bg** 's secondary reflection peaks, and that their position results from simultaneity of:

- a **FP** effect identical to that described in the **P_Bg Band**, predominant outside the secondary 605 reflection peaks of the **Bg**
- another **FP** effect between the **Bg**, which has more and more effect in its secondary reflections, and the multilayer mirror.

Table 4: *FSR* between secondary peaks $\delta\lambda < 0$ of fig. 4.b close to the main peak numbered 0

Pair of peaks (n°)	0-1	1-2	2-3	3-4	4-5
***FSR* (10^{10} Hz)**	10.47	6.57	6.93	7.04	7.04

4.6. Interleaved-Fibre-H-FP (IF-H-FP)

We consider here **H-FPs** similar to those made in [6], which include a length section L_i of non-photosensitized single-mode fibre interposed between the **Bg** and the multilayer mirror. Experimentally, this fibre section is one of the non-photosensitized ends of the fibre in which the **Bg** has been photo-written, cleaved or polished to adjust the L_i length, and abutment or glued with a multilayer mirror deposited on another single mode fibre to achieve an **H-FP**. The results of [6] show that L_i can easily be adjusted experimentally in a satisfactory way: for **IF-H-FP**, it is this adjustment that allows to obtain the desired phase shift between the multilayer and **Bg** periods by a more basic method for a non-multiple **H-FP**, than the adjustment of a layer of the multilayer mirror or a photorefractive correction, but less well adapted to the parallel manufacture of a large number of **H-FP**, or to the construction of a serial multiple **H-FP**. Here, we simulate **IF-H-FP** filters with sinusoidal **Bg**, whose simulation, lighter at all λ, is entirely singlemode in the **Bg**. In [6], a **1D** model was given, where the equivalent length of the **IF-H-FP** to a plane wave **FP** gives is $L_{eq} = L_i$. We will show here that this fits well for $L_i >> L_{Bg}$ by doing a **3D S-matrix** simulation of **IF-H-FP** in order to find the right model also for low values of L_i, and then also for $L_i = 0$.

4.6.1. Observation of the main peak centred at λ_0

The T_{11} ($\delta\lambda$) spectrum **3D** simulations of **IF-H-FP** with Fimmprop show the following behaviour:

- To maintain continuity when $L_i \rightarrow 0$, for the **H** layer at the interface with the **IF**, we keep in the simulations the e_{trim} value adjusted for **H-FP1** and therefore adapted for $L_i = 0$. For $L_i >> L_{Bg}$ (this restriction on L_i is evident according to Eq. 12 demonstrated later in 4.6.3), $L_{Eq} \simeq L_i$ and the only values of L_i, which give $T_{11}(\lambda_0) \simeq 1$, are then such that for the fundamental mode of the interleaved fibre, $L_i = M\ \lambda_0 / (2\ n_{eff})$ with M integer (and where $n_{eff} = 1.4460763$ is the effective index of the fundamental mode of the fibre at λ_0) [11]. The experimenter will prefer to

[11] For example, for **IF-H-FP1**, a 1921 0±.3 variation of M around its integer value 1921 <==> L_i = *1028*.9632µm±0.161µm brings T11(λ_0) below 40%. A polishing accuracy to within a few nanometres is therefore sufficient.

have the thickness e_H instead of e_{trim} for the **H** layer at the interface with the **IF** and will obtain the transmission peaks for (mantissa of M) = 0.5 for $L_i >> L_{Bg}$.

- The larger L_i and M are, the narrower the main peak is (fig. 6). **IF-H-FP** therefore have the advantage of an adjustable and narrower bandwidth, but do not have the robustness of a fixed technology and are sensitive to vibrations if the fibre is buffered and not glued to the multilayer (then well adapted to sensor applications). For the spectrum of **IF-H-FP1** following observations, the description is made with reference to the **R_Bg Band**, **O_Bg Band**, **P_Bg Band** of the incorporated **Bg**.

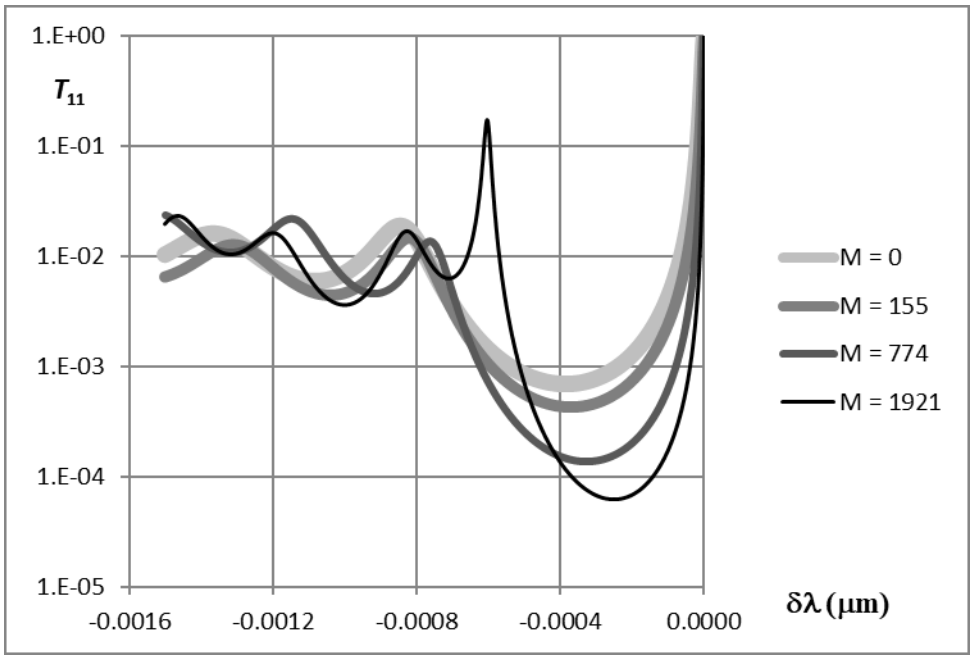

Figure 6: T_{11} (δ_λ) for the **IF-H-FP1** filter with L_i corresponding to the values of M = {0; 155; 774; 1921}. They respectively result in an increasingly narrow transmission peak at $\delta\lambda = 0$, of which only the left part is represented here, the spectrum being almost symmetrical with respect to $\delta\lambda = 0$ for the spectral band represented.

4.6.2. Observations in the P_Bg Band

Small secondary transmission peaks appear in figure 7, but not regularly, spectrally or in amplitude, unlike what was observed for **H-FPs** without **FI** in figure 5. Outside the **Bg** reflection band, we again

assimilate the **Bg** to a homogeneous medium with an average index $n_{eff} + \Delta n/2$. Three mirrors are involved, very thin (**M_1**), or of null thickness (**M_2**, **M_3**):

- **M_1** = multilayer = mirror of almost zero thickness (thickness in the order of λ_0)
- **M_2** = dioptre **FI-Bg**, did not intervene in the **H-FP** without **FI**
- **M_3** = dioptre **Bg-input fibre**

M_1 alone has a high reflection coefficient, while **M_2** and **M_3** have the same tiny reflection coefficient as a Δn/2 step of refractive index dioptre. The phenomena observed for the secondary peaks result from beats between the longitudinal modes of the 3 **FPs** formed by the 3 pairs of mirrors (**M_1-M_2** separated from L_i, **M_2-M_3** separated from L_{BG}, **M_3-M_1** separated from $L_i + L_{BG}$). Since the amplitude of these beats is low (<0.0005 in figure 7 for **IF-H-FP1**), they have no disadvantage or interest for use as a bandpass filter, and their study will not be continued here.

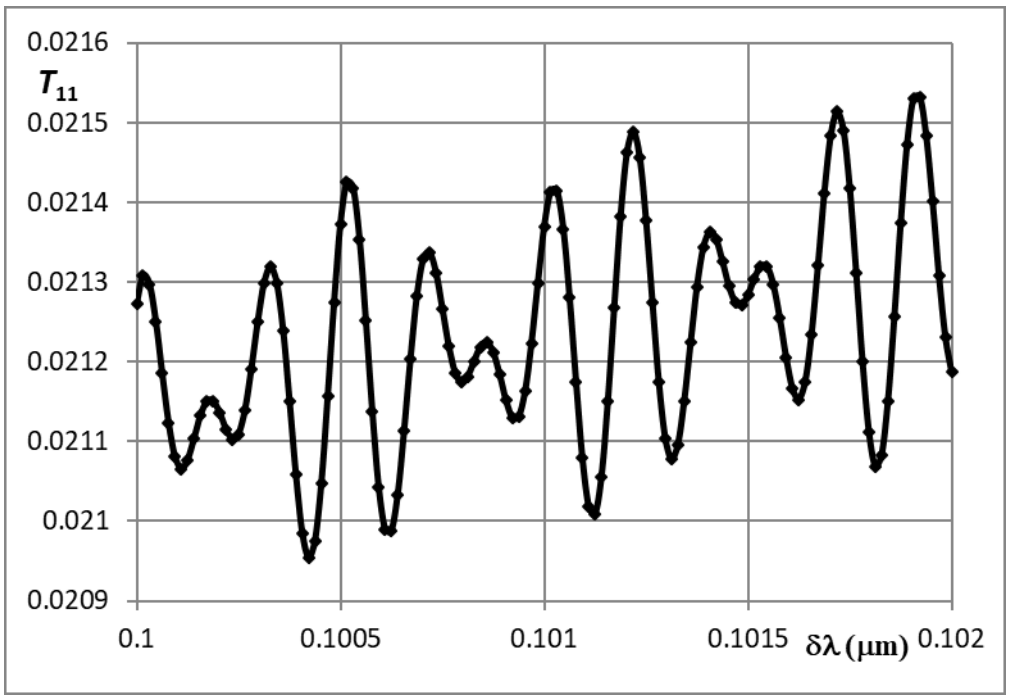

Figure 7: T_{11} ($\delta\lambda$) for the **IF-H-FP1** filter simulated with M = 7464 → $L_i \simeq$ 4.000 mm, showing some secondary transmission peaks in the same spectral band as in figure 5, very far from the **R_Bg band**.

4.6.3. Observations in the R_Bg Band and O_Bg Band

In the **R_Bg Band**, we consider only the reflections between the **Bg** and the Multilayer of reflection coefficients each close to 1 and preponderant, which form an effective cavity whose effects exceed those of all the other pairs of mirrors. These mirrors do not form a classic **FP**, since the **Bg** is a very thick mirror with very narrow reflecting band. The simulation shows that for **IF-H-FP1,** if $L_i > L_{i,Th}$ ($L_{i,Th} = L_i$ Threshold value), secondary peaks appear that are simultaneously in the **R_Bg Band** and become larger than all secondary transmission peaks in the **O_Bg Band** (fig. 6 & 8). For **IF-H-FP1**, we obtain $L_{i,Th}$ = 723.51µm <=> M_{Th} = 1350. The simulations show that this threshold is inversely proportional to Δn. This is because the spectral reflection width of a Bragg grating and therefore that of the super-rejection of an **H-FP** are also, as confirmed by simulations. Given the high value of $L_{i,Th}$ in comparison with polishing accuracy, it is therefore easy to set $L_i < L_{i,Th.}$

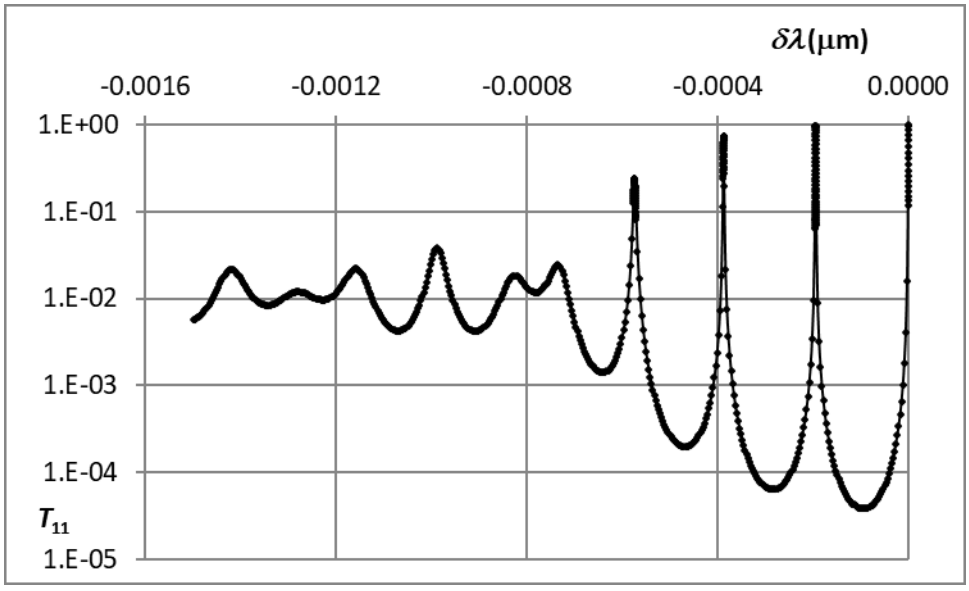

Figure 8: T_{11} ($\delta\lambda$) for **IF-H-FP1-** filter with M = 7464 → $L_i \simeq$ 4.000 mm > $L_{i,Th}$, showing the left half of the main peak on the far right and some secondary transmission peaks. When located in the **H-FP1** super-rejection band, the first secondary transmission peaks are very narrow (this is why a few additional

calculation points have been added to the regular resolution of 513 points to precisely determine their vertex, which shows that the first one here goes back to 100%).

For $L_i > L_{i,Th}$, the simulation shows that for **IF-H-FP1**, secondary peaks appear close to the main transmission peak, exactly equidistant of the FSR of an equivalent conventional FP filled with a uniform medium having the refractive index n_{eff} of the fundamental mode of the fibre SMF28 at λ_0, and of equivalent length:

$$L_{Eq} = L_i + x(R)\,L_{Bg} \qquad \text{(Eq. 12)}$$

with x depending only on R, and $x(R) = 0.179$ for the **IF-H-FP1** filter high L_i values (figure 9). So, L_{Eq} also represents the average length travelled by the fundamental mode passing through the real cavity. To determine x, only the largest values of L_i are considered, as those starting to approach $L_{i,Th}$ only allow to observe a single secondary transmission peak whose position at the boundary between the **R_Bg Band** and **O_Bg Band** is disturbed (fig. 6, 8) by the other **FPs** described in § 4.6.2. Since the value of x appears constant in figure 10 for the large L_i values, we propose to keep the same value of x for all L_i values. Note that this new model, more precise than in [6] where x is zero, is consistent with the experimental observations described qualitatively in [6] for $L_i >> L_{BG}$.

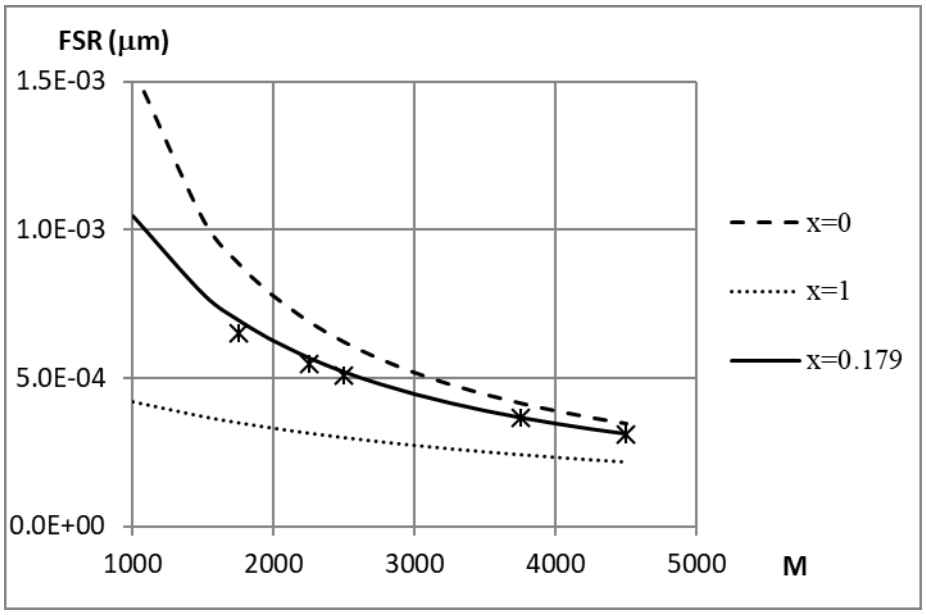

695 **Figure 9:** For **IF-H-FP1**, comparison of the FSR as a function of M simulated with Fimmprop between the main peak and the first neighbour (stars), with the FSR of a conventional **FP** of length $L_{Eq} = L_i + x\, L_{Bg}$, for various values of x. The value $x = 0.179$ allows a good recovery for the large values of M corresponding to large L_i.

The simulation shows that x decreases sharply as the reflection coefficient R of the **H-FP** mirrors
700 increases and approaches 1 (fig 10 where *R of* the multilayer and of the **Bg** depend on N, see table 1; the **IF-Bg-FP** also in figure 10 are discussed later in 4.6.4). We have verified that x does not depend on how R is obtained by choosing the photorefractive variation amplitude Δn of the **Bg**.

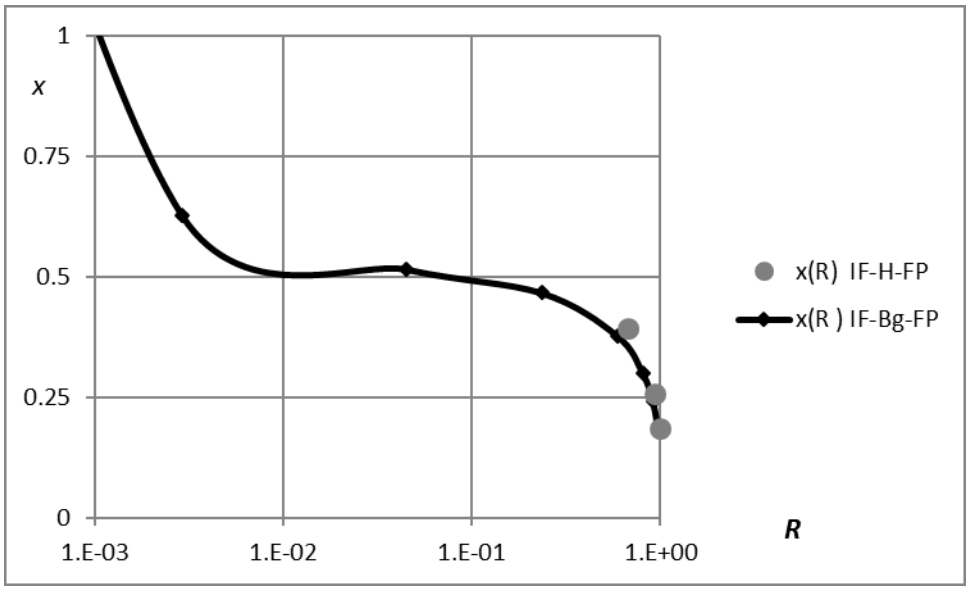

705 **Figure 10:** Dependence of x as a function of the reflection coefficient R of **Bg** for balanced **IF-H-FPs** (with N = 1, 2 or 3), and balanced **IF-Bg-FPs** with various N_{Per} each having M = 3464 <=> $L_i \simeq 1.856$ mm, and sinusoidal **Bg** with $\Delta n = 2\ 10^{-3}$ similarly as for the **IF-H-FPs**. The **IF-H-FP1** filter corresponds to the right-most point of the figure with $R = 0.988$.

4.6.4. Consequences of the equivalent FP model with x independent of L_i

710 It should be emphasized that it was only the extension of Eq. 12 by keeping x invariable for low L_i values that allowed us to estimate the FSR of an **H-FP** without interleaved fibre. The logical

consequences of this model are not in contradiction with numerical simulations, which, without providing perfect quantitative evidence, confirm it as very likely:

- For **H-FP** without **IF**, $L_{Eq} = x\ L_{Bg}$ is then the average length travelled by the fundamental mode passing through the real cavity, and is in good accordance found less than L_{Bg}.

- The FSR of a **H-FP** without **IF** is FSR = c / [$2n_{eff}\ x\ L_{\mathbf{Bg}}$] = 3.182 nm for **H-FP1**, i.e. significantly more than the 0.78 nm half-width of the corresponding **R_Bg band**. Therefore, significant secondary peaks of **FP** resonance between the multilayer and the **Bg** cannot occur. Indeed, the observation of $T_{11}(\delta\lambda)$ for **H-FP1** in Figure 4.b near of $\delta\lambda$ = -FSR shows a weak transmission peak (the 5th secondary peak in the **O_Bg band**). However, this belongs to a group of secondary peaks spaced far less than the FSR, and thus to a different phenomenon, which has already been described in § 4.6.2.

- For **IF-Bg-FP** with the same **Bg's** as an **H-FP**, the validity of our model implies that we must obtain $L_{Eq} = L_i + 2\ x\ L_{Bg}$ with the same value of x as the **IF-H-FP** having even R mirrors and even L_i. This is precisely what is observed with the good overlap of the 2 curves in Figure 10. The **IF-H-FP** simulation only allows access to a small number of R values, given the high step of refractive index in its multilayer. On the other hand, $\Delta n = 2\ 10^{-3}$ being far much lower in the simulated **Bg** than in the multilayer, this allows access by varying N_{Per} to much lower, and much closer together, R values for **IF-Bg-FPs**. The case $R < 10^{-2}$ is not considered, as it does correspond to so weak reflectors, that it makes the usual **FP** calculation inappropriate. For the selected L_i value of fig. 10 and small values $10^{-2} < R < 10^{-1}$, $x(R)$ varies little around 0.5. For $R > 10^{-1}$, $x(R)$ then decreases sharply. Obviously, for **IF-Bg-FP**, in the case R =1, the grating length is infinity, and this leads to $x = 0$ (not represented on the figure because it corresponds to an infinity fineness inaccessible due to manufacturing tolerances and material absorption).

- For **Bg-FP** without **IF**, FSR = c / [$2n_{eff}\ 2\ x\ L_{BG}$] is half that of the **H-FP** with the same **Bg** if we assume that each of the 2 **Bg** corresponds to an average path $x\ L_{Bg}$ by the fundamental mode when crossing the cavity. Consequently, the widening of the main peak due to cavity

losses, which is FSR /F must be double for the **H-FP** than for the **Bg-FP** with the same **Bg** (F is the fineness [19] corresponding to both the **H-FP** and the **Bg-FP** with the same **Bg**). In addition, the width of the simulated peak, which may also have other origins, must be greater than the broadening by cavity losses. Our simulations confirm that the width of the main transmission peak of a balanced **H-FP** is indeed twice that of this peak for the **Bg-FP** with the same **Bg** as this **H-FP**. In addition, in figure 4.b., it appears that the FWHM of the line of the main transmission peak of **H-FP1** is 12.856pm. The calculation of the broadening due to the losses of the equivalent cavity is indeed found to be lower and is 11.705 pm[12]. A plausible interpretation of the small difference is the consequence of the standard deviation of the length of the mean path of the fundamental mode in the cavity around its mean value $x\ L_{Bg}$.

- For **Bg-FPs** without **IF**, the simulations reported in 4.3 show that $\delta\lambda_{Max}$ / δe_{trim} is inversely proportional to Δn. This corresponds perfectly to Eq. 10 & 12. Let us note however that if Eq. 10 allows to find the proportionality of $\delta\ \lambda_{Max}$ to δe_{trim} and the order of magnitude of the proportionality coefficient, it does not allow to find its right value: indeed, in 4.3, Fimmprop gave for **H-FP1** $\delta\ \lambda_{Max}$ /δe_{trim} = 21.09 pm/nm, while Eq. 10 & 12 give $\delta\ \lambda_{Max}$ /δe_{trim} = 14.53 pm/nm. Again, this is because the assumption of a plane wave in the layers used to establish Eq. 10 instead of multimode propagation is inadequate.

4.6.5. Manufacturing tolerances on M and L_i:

For **IF-H-FP1**, for an interleaved fibre SMF28, $L_i = M\ \lambda_0 / (2\ n_{eff})$ with $\lambda_0 / (2\ n_{eff})$ = 0.535932993 µm [13]. When the integer part of M increases, the FWHM $\Delta\lambda$ of the central transmission peak of the **IF-H-FP** decreases significantly as outlined in 4.6.1. The ratio between the shift of the transmission peak $\delta\lambda_{Max}$ and $\Delta\lambda$ depends only on M's mantissa. For small variations of M's mantissa around 0, the main peak degrades little. According to Eq. 8, this peak moves linearly as a function of δL_i. For **IF-H-FP1** and small variations of L_i from $\delta L_i = 0$, the Fimmprop simulation shows that the top of the main peak

[12] For H-FP1 filter, FSR = 3.046 nm. The fineness $F = \pi\ R^{0.5}/(1\text{-}R)$ with at λ_0 the power reflection of the **Bg** ==> R = 0.9880 ==> F = 260.224 ==> FSR/F = 11.705 pm.

[13] This accuracy corresponds to a mantissa accuracy of M corresponding to an uncertainty of +/- 1nm on L_i for M up to 10^6, i.e. $L_i \simeq 0.5$ m

shifts by $\delta\lambda_{Max}/\delta L_i$ = +6.28pm/nm. For the adjustment of the **H** layer of **H-FP1** Fimmprop simulation in 3.3, we found $\delta\lambda_{Max}/\delta e_{trim}$ = 21.09pm/nm, or 3.36 times more, which rendered the adjustment significantly more difficult in this case. This ratio should be compared with the ratio of the effective indices in the **H** layer (multimode certainly, but with effective indices each very close to 3.479 for the first dominant modes), and the effective index of the single-mode fibre $n_{eff} \simeq 1.446$, i.e. a different ratio of 2.41 with the same calculation accuracy. But it suggests that using a low refractive index like SiO_2 at the interface renders the adaptation easier. Finally, it should not be forgotten that according to Eq. 8, $\delta\lambda_{Max}/\delta L_i$ varies considerably according to L_i and so to M. This is observed in figure 11 where the calculation made from Eq. 8 & 12 also shows a perfect coincidence with the shifts of the main transmission peak of **IF-H-FP1** simulated by Fimmprop in function of the integer part of M. The calculation of figure 11 is made with x = 0.174 (very close to the value x = 0.179 retained above) and a mantissa of each M corresponding to δL_i =1 nm.

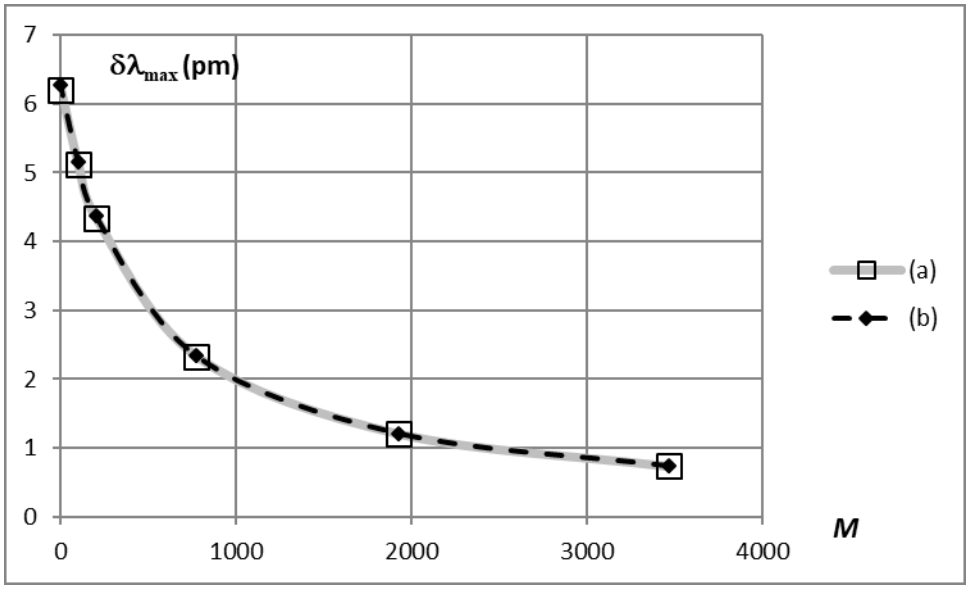

Figure 11: For ΔL_i = + 1nm <=> ΔM = + *0*.00187, shift $\delta\lambda_{Max}$ of the main peak of **IF-H-FP1** as a function of the integer part of M:

a) Calculated with Eq. 8 & 12 for x = 0.174

b) According to the displacement with M of the peak top simulated by Fimmprop

5. Discussion

5.1. Modelling

The **3D S**-matrix simulations allowed us to check that only certain assumptions of the **1D** simulation model by **CMMS** presented in [1] are verified and only in some cases for **H-FP** without **IF**:

- Only a multimode calculation by **S**-matrix in the layers can find the correct values of e_{trim} and $\delta\lambda_{Max}$ /δe_{trim} order of magnitude. We have shown that the experimenter can find himself e_{trim}, which corresponds to a minimum of reflection of the filter during the deposition of the boundary layer with the interface. Nevertheless, the knowledge of this thickness by numerical simulation helps the experimenter to develop his process.

- A single-mode calculation in the **Bg** can only be performed for the **H-FP** with sinusoidal **Bg** even at optical resonance, and for **H-FP** with sharp step **Bg** outside resonance only.

For **BG-FPs**, there are no thin layers, and a single mode calculation in the fibre and in the **Bg** is possible, excepted at resonance in the case of sharp step **Bg**.

For **IF-H-FP**, the phase shift is set in the **IF**, which is single mode, so a single mode calculation can easily find the right fibre length to adjust the phase shift of the mirrors, and this length can easily be retouched afterwards, unlike the thickness of the adjusted interface layer of **H-FPs** without **IF**. So a single mode **1D** calculation is sufficient, except at resonance in the case of sharp step **Bg**.

Since the **CMSS** requires knowledge of the effective fibre indices, which are not calculated by common thin-film software, it is however preferable in all case to make all calculations with software such as Fimmwave/Fimmprop, which calculate fibre modes as well as **S-matrix** propagation, and have great programming flexibility to optimize sampling, thanks to their "adiabatic taper" algorithm.

To obtain balanced **H-FPs** whose transmission is 100% at the centre wavelength, the number of periods in the **Bg** must be carefully adjusted. For a given multilayer in the **H-FP**, this results in a smaller number of **Bg** periods and a narrower **H-FP** bandwidth in the case of a step longitudinal

profile **Bg** than a sinusoidal one. The discrete appearance of the **Bg** reflection coefficient according to its number of periods can prevent the transmission of the **H-FP** from increasing exactly to 100%, as more as the **Bg** index step is high.

The considerably wider rejection band for **H-FPs** than for **Bg-FP** reported in [1] has been studied here more fully. Around the transmission peak of the **H-FP**, there is a stronger rejection band whose spectral width corresponds to the reflection band of the **Bg**. Beyond that, the rejection, less strong, corresponds mainly to the reflection coefficient of the multilayer, however lightly degraded by very low secondary transmission peaks studied in detail here.

The study of strong **FP** oscillation (fig. 8) appearing in the reflecting band of **IF-H-FP** with $L_{i,Th} \leq L_i \leq$ some L_{Bg} allowed to develop a new equivalent cavity model of length $L_{EQ} = L_i + x\, L_{Bg}$ for the **IF-H-FP** and $L_{EQ} = L_i + 2\, x\, L_{Bg}$ for the **IF-Bg-FP**, where x depends only on the assumed reflection coefficient common to all mirrors (fig. 10). The trick to determine x for **H-FP** or **Bg-FP** without **FI** is to determine it for long lengths of interleaved fibre where x varies little (not too long either so as not to produce too sharp resonances that would disturb the calculations, and not to short so as those resonances do not vanish in the secondary transmission speaks studied earlier in the rejection band). Keeping this x-value for $L_i = 0$, where it cannot be determined otherwise, allows an excellent quantitative analysis of the line width of **H-FP** and **Bg-FP** taking into account their fineness, and to explain why the line width of the main transmission peak of a balanced **H-FP** is twice that of a **Bg-FP** whose **Bg** have the same reflection.

All these elements will help in the study of serial multiple **H-FPs** to be presented in detail in a later publication, which, like for bulk substrate **M-FPs,** simultaneously improve the rejection and spectral profile of the transmission peak of a single **H-FP**, but with more demanding manufacturing tolerances.

5.2. Performance and applications

The **3D** simulation of single **H-FP** shows that unlike **M-FPs** with the same Fineness between single-mode narrow core fibres, they exhibit no diffraction in the multilayer. In opposition, diffraction only allowed passbands of 2 to 3 nm for fibred **M-FPs**, and 0.1 nm for **M-FPs** on bulk, and for

sophisticated fibred **M-FPs** presented in [10]. But since the latter are difficult to achieve, non-multiple **H-FPs** are the simplest fully fibred filters to achieve for bandwidths from 15 fm, to 2 to 3 nm. This is very exciting, but the biggest difficulty with these filters is controlling the position of their pass wavelength λ_{max} at which they have maximum transmission as a function of the phase adjustment of their mirror periods. We have shown that $[\delta\lambda_{max}/\delta e_{trim}]/FWHM$ is independent of Δn.

For an included **(HL)^{3}H** Si/SiO_2 multilayer, the use of deposition to the atomic layer accuracy alone therefore leads at best to respective accuracies of $\delta\lambda_{max}/FWHM = 38.3\%$ for equilibrated **H-FP** filters and 11.49% for an equilibrated **IF-H-FP** near $L_i = 0$. This is insufficient for many applications, unless by chance the thickness grid accessible by atomic layer adjustment just happens to fall on the right value, or the filters are retouched one by one by photo-refractivity. Improving these results for mass production would require another publication focused on this subject, and of a mainly experimental nature, for which we suggest here only a few leads:

- A multilayer mirror terminated with a very high refractive index Si **H** matching layer gave us a very compact multilayer mirror and a fairly optimal multilayer reflection value. But the somewhat better result with polishing the interleaved silica fibre of lower refractive index suggests that the use of multi-layer mirrors terminated with SiO_2 or other low refractive index **L** material may allow somewhat better phase matching accuracy.

- In the same vein, it could be tried to dope the matching layer during its deposition, so that the available optical thickness grid is shifted when setting the thickness to the nearest atomic layer, so that the right value can be better achieved. Ion plating technology can work on this principle.

- In the case of mirrors produced by integrated optics photolithography, an experimental approach specific to each technology chosen is of course essential. It must also be considered that **Bg** with $\Delta n = 2\ 10^{-6}$ and the same reflection at λ_0 than for **H-FP1** would be more than 1m long, which is not a problem for fibres, but for integrated optics it is, as it would require for example over 100 folding of the grating inside a 1 cm^2 square circuit.

For the same internal multilayer mirror and **Bg**, interleaved fibre filters have a narrower main bandwidth, and it is easy to obtain a bandpass filter with a single bandwidth since it is sufficient for the interleaved fibre length to be under just over 700 μm for the **IF-H-FP** considered, and half for **IF-Bg-FP**.

From the point of view of their performance requirements, **FP** applications as bandpass filters with broad rejection band fall into two categories:

- The most demanding require control of the absolute bandwidth position
    - Signal applications: DWDM filtering for telecommunications (typical bandwidths 400, 200 or 100 pm until now [20]).
    - Spectrally absolute sensors: e.g. filtering of Raman Lidar Stokes and anti-stokes responses, filtering of fluorescence lines...
- Spectrally relative sensors for which only the displacement of the bandwidth following a variation of the mesurande is measured, only require that the bandwidth exists, but do not fix its position in an absolute way (e.g. pressure and/or distance sensor obtained by an air gap between the **FP** mirrors). On the other hand, these sensors require calibration.

Thus, it can be seen that fibre-optimised or integrated **H-FPs** with bandwidths as narrow as 15 fm and with a rejection of several hundred nanometres would greatly expand the possible applications.

For DWDM, it would become fully fibred on the one hand, and on the other hand, it would allow fine spectral processing within a metropolitan telecommunications network. Allowing spectral sorting with narrower bandwidths better suited to single subscriber selection as suggested in [21], this could increase the number of DWDM filters placed at the subscriber's premises and thus their market. However, for such applications leading to the manufacture of very large series of components, solving the phase matching tuning difficulty by front-end parallel processing is essential. On the other hand, relative sensor applications see their possibilities immediately increased considerably, as well as certain absolute sensors if they are manufactured in small numbers and if, in exchange for an increase in price, the individual adjustment of their phase matching, for example by photo-refraction, is acceptable with respect to their market (in this case, **IF-H-FP** can be more flexible to realise, but less stable over time).

6. Conclusion

Despite they are partially constructed with un-guiding layers, the modal **3D** simulation of hybrid **FP** shows no diffraction, and the absorption effects are also negligible, both in opposition to multilayer **FP** between narrow core fibres. Their **3D** simulation by **S**-matrix, which is highly multimodal in the layers, is essential in the case of **H-FPs** without interposed fibre to find the thickness of the layer at the interface with the grating. Once this has been found, and also for **H-FPs** with interleaved fibre or purely in **Bg**, their multimodal simulation in the grating is only indispensable at the top of their transmission peak, only in the case where their grating has a sharp step axial refractive index profile. Their very broad and large rejection, far wider than that of **BG-FP,** is similar to that of their multilayer mirror (with weak oscillations studied precisely here), except in the main reflection band of their **Bg** where it is much stronger. The control of the layer thickness at the interface is not critical for the collapse of a peak broader than 15 fm, but is critical for controlling its shift. So, 15 fm passband filters can be obtained for individual devices and also industrially for spectrally relative sensors. But applications with an absolutely fixed wavelength and requiring large industrial production such as DWDM require an experimental research effort in each chosen technology for a better control of the passband shift, and passband of 1.5 pm to 150 fm would be more realistic for integrated optics because of the grating length. Every small spectral oscillations appearing in the rejection band of the **H-FP** have been accurately observed and interpreted. The simulation of hybrids with interleaved fibre between mirrors allows us to show for certain properties the equivalence of a hybrid without interleaved fibre with a **FP** travelled by plane waves and with localized mirrors, having for length a fraction that we have determined of the length of their **Bg**. The same is true for all properties of a **FP** with 2 **Bg** identical to that of the hybrid, where the equivalent cavity length is found to be double.

Appendix A: Formalism for plane waves FP interferometers

The intensity transmission of a **FP** is expressed as a function of its Airy transmission [20], which is:

$$T_A = \frac{1}{(1-m)^2 + 4m\sin^2(\varphi/2)} \qquad \text{(Eq. A1)}$$

As they will be proved to have negligible effect here, we will not consider losses by absorption, and the loss factor is therefore $m = r_1\, r_2$ where r_1, r_2 are the amplitude reflection coefficients of the mirrors; we will also consider R_1, R_2 the intensity reflection coefficients and t_1, t_2, T_1, T_2 the amplitude and intensity transmission coefficients of these mirrors. The transmission in intensity of the **FP** is then $T = T_1\, T_A\, T_2$. We will often consider for the cavity equivalent to a single mode propagation between 2 ultra-thin mirrors, the phase φ of a round trip in the cavity, which is:

$$\varphi = 2kL = 2\, n_{eff}\, (2\pi\, f\, /\, c)\, L_{Eq} \qquad \text{(Eq. A2)}$$

where k is the wave vector in the cavity, f is the frequency and L_{Eq} is the equivalent length of the cavity filled with n_{eff}. For $\varphi = 2\, p\, \pi$ and for $\varphi = (2p+1)\, \pi$ where p is a natural integer, the maximum and minimum transmission values are obtained respectively:

$$T_{\max} = \frac{1}{(1-m)^2} T_1 T_2 \quad \text{(Eq. A3)} \qquad \text{and} \qquad T_{\min} = \frac{1}{(1+m)^2} T_1 T_2 \quad \text{(Eq. A4)}$$

The extreme transmissions of the cavity $T_{\max}$ and $T_{\min}$ can be easily specified after limited development calculations in some particular cases that will facilitate our reasoning following the simulations, and for which mirrors transmissions $T_1 T_2 = |t_1|^2\, |t_2|^2$ if we consider identical media on each side of the FP:

- For 2 identical mirrors with reflection coefficients $R_2 = R_1$ close to 1, since then the loss factor $m \simeq R_1$ and $T_1 = 1\text{-}R_1$, we find $T_{\max} = 1$ and $T_{\min} = T_1^2/4$.

- For one mirror $R_1 \simeq 1$ and the other mirror $R_2 \simeq 0$, since then $m \simeq r_2$ reflection amplitude and $T_2 \simeq 1$, we find values close to T_1, which are:

$$T_{\max} \simeq T_1 (1 + 2r_2) \quad \text{(Eq. A5)} \qquad \text{and} \qquad T_{\min} \simeq T_1 (1 - 2r_2) \quad \text{(Eq. A6)}$$

T_A has a transmission peak each time sin (φ/2) = 0, which is obtained at the frequencies

$$f = p\frac{c}{2n_{\text{eff}}L_{Eq}} \Leftrightarrow \lambda_v = \frac{c}{f} = \frac{2n_{\text{eff}}L_{Eq}}{p} \qquad \text{(Eq. A7)}$$

where p is the interference order, and λ_v is the wavelength in the vacuum of the top of the transmission peak (p_0 is the order for $\lambda_v = \lambda_0$). We deduce that if the length of the cavity changes from L to $L' = L + \delta L$, the wavelength of the Airy peak of order p is translated proportionally to L of the value:

$$\delta\lambda_v = \frac{2n_{\text{eff}}\delta L_{Eq}}{p} = \lambda_v\frac{\delta L_{Eq}}{L_{Eq}} \qquad \text{(Eq. A8)}$$

A variation in the thickness of the **H**-layer next to the **Bg** introduces a phase term to the reflection coefficient of the multilayer mirror, which can no longer be considered real. Here we make the approximation that the beam is a plane wave in the H-layer. This phase shift can then be represented by a thickness e'_{trim} of material **H**. Thus, Eq. A2 becomes:

$$\varphi = 2\,n_{eff}\,(2\pi f\,/\,c)\,L + 2\,n_H\,(2\pi f\,/\,c)\,e'_{trim} \qquad \text{(Eq. A9)}$$

This thickness can always be written as $e'_{\text{trim}} = e_0 + e_{\text{trim}}$, where e_0 is a constant thickness whose value does not matter: so, $\delta e'_{\text{trim}} = \delta e_{\text{trim}}$. The Airy peaks correspond to λ_V such that sin (φ) = 0, i.e.:

$$\lambda_V = \frac{2n_{eff}L_{Eq} + 2n_H e'_{trim}}{p} \Rightarrow \frac{1}{p} = \frac{\lambda_V}{2n_{eff}L_{Eq} + 2n_H e'_{trim}} \qquad \text{(Eq. A10)}$$

For a fixed p-order peak, it comes:

$$\delta\lambda_V = \frac{2n_H\delta e'_{trim}}{p} = \frac{2n_H\delta e_{trim}\lambda_V}{2n_{eff}L_{Eq} + 2n_H e'_{trim}} \simeq \frac{n_H\lambda_V}{n_{eff}L_{Eq}}\delta e_{trim} \qquad \text{(Eq. A11)}$$

References

1. J. Bittebierre, B. Lazaridès, Narrow hybrid bandpass filters with broad rejection band for singlemode waveguides, Applied Optics, 40 (2001) 11-19

2. J. Bittebierre, B. Lazaridès, Bicorne filters for singlemode waveguides, Applied Optics, 40 (2001) 5028-5033

3. J. Bittebierre, B. Lazaridès, Hybrid filters with chirped gratings for DWDM applications, Proceedings of Photorefractive effects, materials and devices, Nice, 2003

4. J. Lumeau, M. Cathelinaud, J. Bittebierre, M. Lequime, Narrow bandpass hybrid filter with wide rejection band, Proceedings of Optical Interference Coatings, USA, 2004

5. J. Lumeau, M. Cathelinaud, J. Bittebierre, and M. Lequime, Ultranarrow bandpass hybrid filter with wide rejection band, Applied Optics, 45 (2006) 1328-1332

6. Y. Sano, M. Kobayashi, T. Yosh, Sideband-suppressed narrow bandpass fibre Fabry-Perot filter composed of fibre Bragg grating and dielectric mirror Electronics Letters 49 (2013) 1350-1351

7. A. Thelen, Design of optical interference coatings, Mc Graw Hill, New-York, 1989

8. H.A. Mac Leod, Thin film optical filters, Institute of Physics Publishing, Bristol and Philadelphia, 2001

9. J. Bittebierre, Three-dimensional simulation of diffraction and absorption losses in all-fibre multilayer filters, Applied Optics, 47. (2008) C13-24

10. J. Bittebierre, Reduction of the diffraction in strongly resonant thin-film Fabry-Perot filters between single-mode fibres, Applied Optics, 52 (2013) 3645-3654

11. M. Lancry, B. Poumellec, V. Bengin, P. Niay, M. Douay, C Depecker, and P. J. Cordier, Mechanism of photosensitivity enhancement in OH-flooded standard Germanosilicate perform plates, J. Non-Cryst. Solids 353 (2007) 69–76

12. S. Tisserand, F. Flory, A. Gatto, “Titanium implantation in bulk and thin film amorphous silica”, J. Appl. Phys. 83 (1998) 1-4

13. F. Bakhti, P. Sansonetti, Design and realisation of multiple quarter-wave phase shifts UV-written band-pass filters in optical fibres JLT 15 (1997) 1433-1437

14. P. Biensman, Rigorous and efficient modelling of wavelength scale photonic components, PhD thesis, Information technology dept. of university of Gent, Belgium, 2001

15. D. F. G. Gallagher, T. P. Felici, Eigenmode expansion methods for simulation of optical propagation in photonics: pros and cons, Proc. SPIE 4987 (2003) 69-82

16. G. Metzl, W. W. Morey and W. H. Glenn, Formation of Bragg gratings in optical fibres by transverse holographic method, Optics Letters 14 (1989) 823-825

17. M. Vignaux, F. Lemarchand, C. Grezes-Besset, J. Lumeau, In situ optical monitoring of Fabry-Pérot multilayer structures: analysis of current techniques and optimized procedures, Optics Express, 25 (2017) 18040-18055.

18. M. Varasi C Misiano C. Mancini P. Sartori, Plasma assisted ion plating deposition of optical thin films for coatings and integrated optical applications, Vacuum, 36 (1986) 143-147

19. B.E.A. Saleh, M.C. Teich, Fundamentals of Photonics, Wiley, 1991

20. Spectral grids for WDM applications: DWDM frequency grid; ITU Recommendation G.694.1;. https://www.itu.int/rec/T-REC-G.694.1-202010-I/en ,2020 (accessed 6 June 2021)

21. J. Bittebierre, B. Lazaridès, Filtres à bande passante étroite et à large réjection pour guides d’ondes monomodes : applications aux télécommunications, Proc. Optix, Marseille, France, 2001